MICROCOPY RESOLUTION TEST CHART
NATIONAL BUREAU OF STANDARDS-1963-A

RADC-TR-84-225
Final Technical Report
March 1985

CYLINDRICAL LENS-ARRAY ANTENNA FOR WIDEBAND ELECTRONIC SCANNING

Hazeltine Corporation

E. M. Newman
C. M. Ruskowski

APPROVED FOR PUBLIC RELEASE; DISTRIBUTION UNLIMITED

DTIC
ELECTE
JUN 27 1985
B

ROME AIR DEVELOPMENT CENTER
Air Force Systems Command
Griffiss Air Force Base, NY 13441-5700

AD-A156 085

DTIC FILE COPY

85 06 10 104

This report has been reviewed by the RADC Public Affairs Office (PA) and is releasable to the National Technical Information Service (NTIS). At NTIS it will be releasable to the general public, including foreign nations.

RADC-TR-84-225 has been reviewed and is approved for publication.

APPROVED: *[signature]*

PETER R. FRANCHI
Project Engineer

APPROVED: *[signature]*

ALLAN C. SCHELL
Chief, Electromagnetic Sciences Division

FOR THE COMMANDER: *[signature]*

JOHN A. RITZ
Acting Chief, Plans Office

REPORT DOCUMENTATION PAGE

1a. REPORT SECURITY CLASSIFICATION	1b. RESTRICTIVE MARKINGS
UNCLASSIFIED	N/A

2a. SECURITY CLASSIFICATION AUTHORITY	3. DISTRIBUTION/AVAILABILITY OF REPORT
N/A	Approved for public release; distribution unlimited.
2b. DECLASSIFICATION/DOWNGRADING SCHEDULE	
N/A	

4. PERFORMING ORGANIZATION REPORT NUMBER(S)	5. MONITORING ORGANIZATION REPORT NUMBER(S)
6546	RADC-TR-84-225

6a. NAME OF PERFORMING ORGANIZATION	6b. OFFICE SYMBOL (If applicable)	7a. NAME OF MONITORING ORGANIZATION
Hazeltine Corporation		Rome Air Development Center (EEAA)

6c. ADDRESS (City, State and ZIP Code)	7b. ADDRESS (City, State and ZIP Code)
Greenlawn NY 11740	Hanscom AFB MA 01731

8a. NAME OF FUNDING/SPONSORING ORGANIZATION	8b. OFFICE SYMBOL (If applicable)	9. PROCUREMENT INSTRUMENT IDENTIFICATION NUMBER
Rome Air Development Center	(EEAA)	F19628-80-C-0110

8c. ADDRESS (City, State and ZIP Code)	10. SOURCE OF FUNDING NOS.			
Hanscom AFB MA 01731	PROGRAM ELEMENT NO.	PROJECT NO.	TASK NO.	WORK UNIT NO.
	62702F	4600	14	58

11. TITLE (Include Security Classification)
CYLINDRICAL LENS-ARRAY ANTENNA FOR WIDEBAND ELECTRONIC SCANNING

12. PERSONAL AUTHOR(S)
E. M. Newman, C. M. Ruskowski

13a. TYPE OF REPORT	13b. TIME COVERED	14. DATE OF REPORT (Yr., Mo., Day)	15. PAGE COUNT
Final	FROM Oct 81 TO Jun 84	March 1985	156

16. SUPPLEMENTARY NOTATION
N/A

17. COSATI CODES			18. SUBJECT TERMS (Continue on reverse if necessary and identify by block number)
FIELD	GROUP	SUB. GR.	Cylindrical Lens Array Wide Angle Scanning Array
09	05		Wideband Array
17	09		

19. ABSTRACT (Continue on reverse if necessary and identify by block number)

This report describes the fabrication and testing of a lens antenna that is designed to have wideband scanning capabilities for wide angle scanning in any plane. The lens has a 30 by 40 wavelength aperture. Far field patterns were measured in both the azimuth and elevation planes over an eleven percent bandwidth. The azimuth scan angles were 0°, 15°, 30°, and 45° and the elevation angles 0° and 15°.

The quality of the patterns is fairly good with the average power level from +50° to -50° close to 44 dB in the sidelobe region (excluding the 7 or 8 close in sidelobes). These lobes have peak values about 30 dB.

20. DISTRIBUTION/AVAILABILITY OF ABSTRACT	21. ABSTRACT SECURITY CLASSIFICATION
UNCLASSIFIED/UNLIMITED ☒ SAME AS RPT. ☐ DTIC USERS ☐	UNCLASSIFIED

22a. NAME OF RESPONSIBLE INDIVIDUAL	22b. TELEPHONE NUMBER (Include Area Code)	22c. OFFICE SYMBOL
Peter R. Franchi	(617) 861-3067	RADC (EEAA)

DD FORM 1473, 83 APR   EDITION OF 1 JAN 73 IS OBSOLETE.

TABLE OF CONTENTS

LIST OF FIGURES

SECTION I

INTRODUCTION

1.1 GENERAL

A cylindrical-lens phased-array antenna offers the capability for electronically scanning a narrow pencil beam over wide angles in two dimensions, and for handling wide signal bandwidths without using variable time-delay devices.

An investigation of such a lens-array antenna has been conducted by Hazeltine for RADC/EEA. The first part of the program involves the study of the antenna and design of a specific configuration. The second part of the program included the fabrication and test of a lens-array antenna having an aperture of at least 40 x 30 wavelengths.

This final report presents the results obtained in the second part of the program. The results of the study have been documented in an interim report[1]. The balance of this section will present a brief summary of the antenna concept, and design objectives. Section II presents an overview of the lens configuration which was selected for fabrication. It presents a description of the antenna system and calculated patterns of the antenna. Section III describes the detailed design of the component parts of the lens antenna, including the components for the lens and the line feed which illuminates the lens.

Section IV provides a physical description of the lens antenna and its components. Section V presents the measured array performance, including representative pattern and gain measurements . Sections VI and VII describe some refinements made to the lens in order to improve its sidelobe performance, and the result of tests performed after the modifications. Finally, Section VIII presents a summary and conclusions.

1 P. W. Hannan, E. M. Newman, "Study and Design of a Cylindrical Lens Array Antenna for Wideband Electronic Scanning" RADC-TR-83-128, Dec., 1983.

1.2 ANTENNA DESIGN OBJECTIVES

The purpose of the program was to study and demonstrate the feasibility of using a cylindrical constrained lens for wideband radar systems.

The constrained lens was to achieve the following performance objectives:

Scan:	$\pm 45^{\circ}$ Az.
	$\pm 25^{\circ}$ El.
Total Bandwidth:	5.0 to 5.6 GHz
Instantaneous Bandwidth:	400 MHz
Directive Gain:	38 dB minimum
Aperture Size:	40λ Azimuth
	30λ Elevation
Sidelobes (El):	−28 dB peak
(Az):	−32 dB peak
	6 above −42dB
	4 above −37dB
	2 at −32 dB
	all others below −50 dB
Polarization:	Linear

The hardware to be constructed included the printed circuit lens (without phase shifters) and a single line feed. The line feed was to be scanned in elevation to a single angle (15°) by inserting fixed line lengths in the feed.

SECTION II

LENS-ARRAY ANTENNA OVERVIEW

2.1 THE BASIC ANTENNA

A fundamental approach for a constrained cylindrical-lens antenna
has been derived by Rotman and Franchi (Refs 2, 3, 4). The
three-dimensional cylindrical lens comprises a stacked set of
identical two-dimensional lenses. Each two-dimensional lens
consists of two arrays of radiators interconnected by
transmission lines. This configuration is shown in figure 2-1.

There are four degrees of freedom in the design of such a lens:
the inner contour, the outer contour, the relative location of
the inner and outer array elements, and the lengths of the
interconnecting transmission lines. Rotman and Franchi (refs 2,
3, 4) derive a lens design in which the first three of these
degrees of freedom are used to provide three points of perfect
focusing in the azimuth plane. At azimuth angles between these
three directions the focusing may be imperfect but may still be
quite satisfactory.

Ref 2-   W. Rotman and P. Franchi, "Cylindrical Microwave Lens
         Antenna for Wideband Scanning Applications", Exhibit A in
         ESD RFP F19628-80-R-0077; November 1979.

Ref 3-   P. Franchi, N. Kernweis, W. Rotman, "Wideband Microwave
         Lens Antenna for Tactical Radar Applications",
         Proceedings of 1980 Antenna Applications Symposium,
         Allerton Park, Illinois; September 1980.

Ref 4-   W. Rotman et al, "Cylindrical Microwave Lens Antenna for
         Wideband Scanning Applications", AD-DOO8526; February
         1981.

CYLINDRICAL
LENS OF
STACKED 2-D
LENSES

ONE
2-D
LENS

INNER
ARRAY
SURFACE

OUTER
ARRAY
SURFACE

TRANSMISSION
LINES
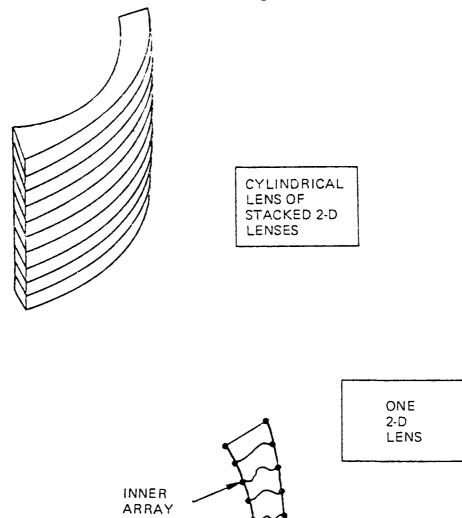
Figure 2-1. Cylindrical Lens Configuration

Figure 2-10.   Azimuth Pattern of Lens Antenna at
5.6 GHz for θ = 0

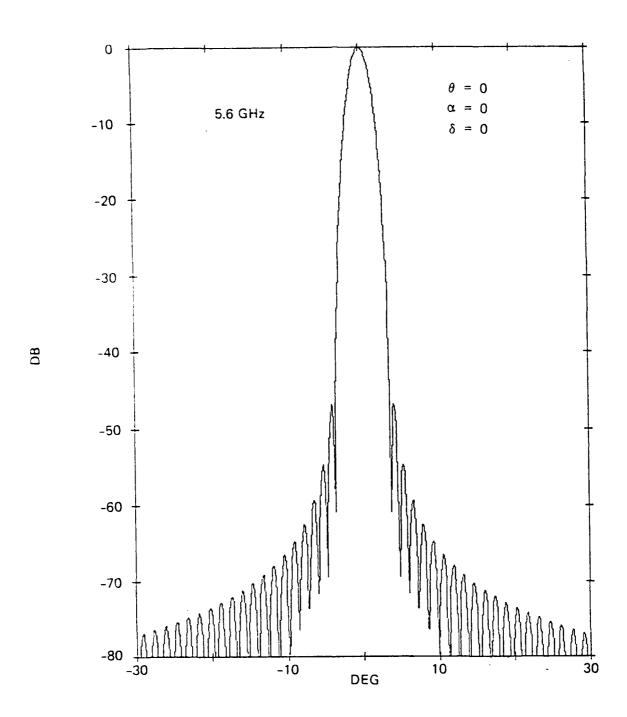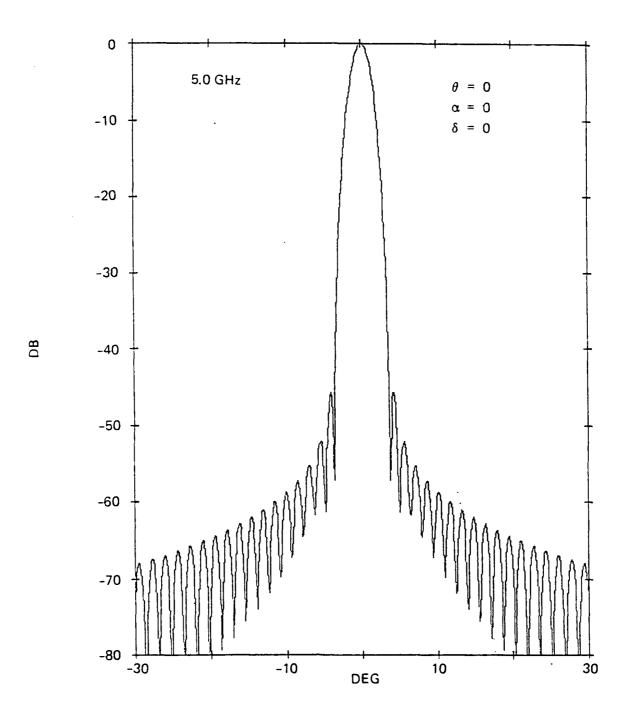Figure 2-9. Azimuth Pattern of Lens Antenna at
5.0 GHz for θ = 0
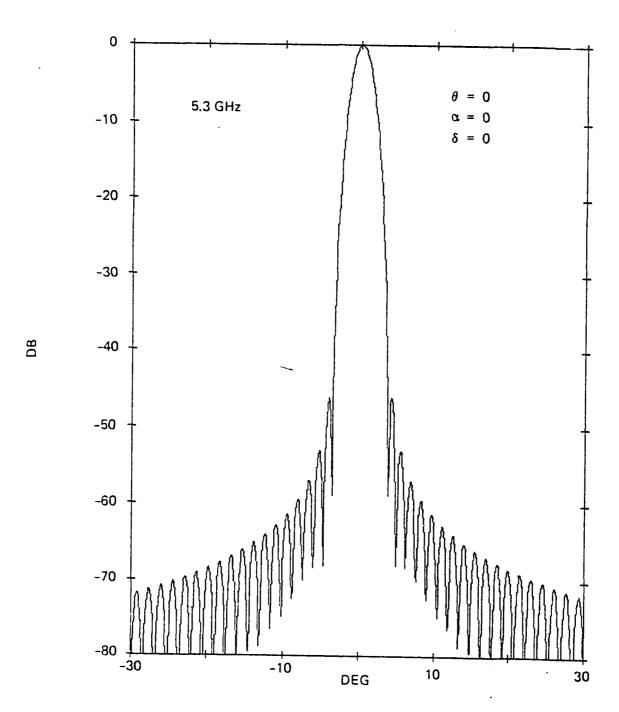
Figure 2-8. Azimuth Pattern of Lens Antenna at
5.3 GHz for θ = 0
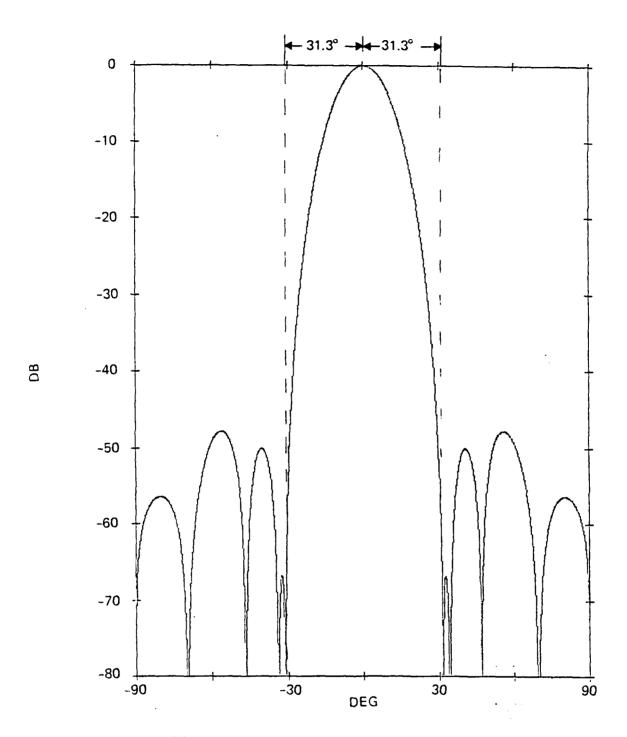
Figure 2-7.   Line Feed Azimuth Pattern
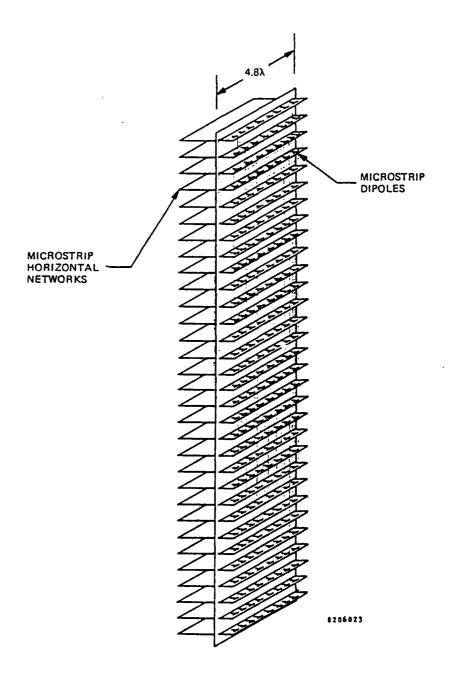
Figure 2-6.   Line Feed Array Configuration

The desired illumination of the lens was accomplished by using eight dipoles in azimuth on the line feed, with the dipole excitations adjusted to provide the required azimuth pattern. Figure 2-6 shows the configuration of the feed array. The eight dipoles are printed on a card along with their associated power divider. The dipoles radiate horizontal polarization, which was selected for the lens.

2.5 CALCULATED ANTENNA PERFORMANCE

The dipole excitation results in the computed feed pattern shown in figure 2-7. At the feed half-angle of 31.3° the feed pattern is quite weak, yielding an illumination of the lens that is almost completely tapered at the sides. The sidelobes of the computed feed pattern are low enough that their contribution to antenna pattern sidelobes is not substantial.

The performance of the array was calculated during the initial study effort for a variety of frequencies and scanned conditions. A few of the patterns presented in the interim report are repeated here in order to provide some indication of the antenna's theoretical performance. The patterns presented here do not include the effects of tolerances, mutual coupling or multiple reflections. These are considered in detail in the interim report.

A computed on-axis antenna azimuth pattern is shown for 5.3 GHz (midband) in figure 2-8 . The sidelobes are at least 10 dB below the sidelobe envelope defined by RADC, leaving a reasonable margin for fabrication tolerance errors. The beamwidth is 2.3°.

The computed effects of operation at the ends of the 5.0 to 5.6 GHz frequency band are shown in figures 2-9 and 2-10. It is assumed that the feed excitation (figure 2-4) remains constant across the band. The beamwidth of the feed pattern changes with frequency but, because of the highly tapered lens illumination, this change has little effect on the azimuth sidelobes of the antenna.

Top View

Side View

D = 40λ
= 7.5 FT

$\frac{F}{D}$ = 0.96

L_f= 35λ
= 6.5 FT

$L_\ell \geq L_f$
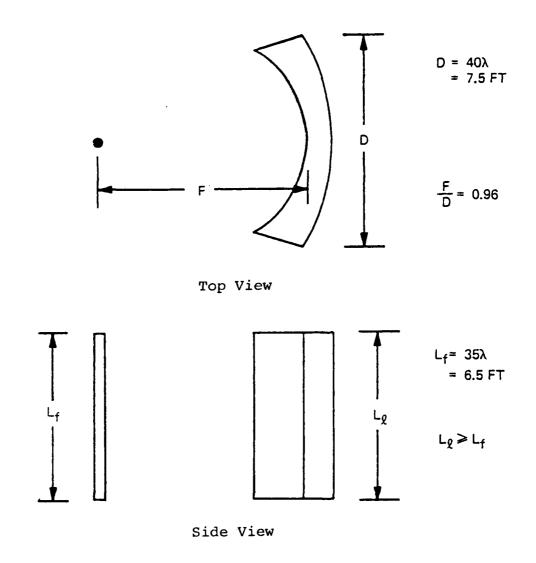
Figure 2-5.   Basic Antenna Configuration.

2-10

degraded by the spillover. The feed radiation must be confined
within the sector ±∅f, the half-angle subtended by the vertex and
the edge of the lens. With an R-2R lens, it can be shown that:

$$\emptyset_f = \text{arc sin } h_{max}$$

$$\text{where } h_{max} = \frac{D}{2F} = .52$$

$$\emptyset_f = 31.3^{\circ}$$

It can also be shown that with an R-2R lens, this half-angle
remains invariant as the feed is moved around the feed arc.

2.2 LENS CONFIGURATION SELECTED FOR FABRICATION

The first phase of the program included a study of several different lens shapes which could be designed using the constrained lens concept. These were termed "dimpled, pointed, hybrid and R-2R". All had a minimum of three azimuth focal points, with the limiting case being the R-2R configuration, which had perfect focusing over the entire azimuth arc.

The R-2R configuration was selected for fabrication based upon:

1. The continuous focused feed arc.

2. The relatively simple geometry.

3. The lack of discontinuities at the center of the lens.

4 The symmetry of the lens.

2.3 LENS CONFIGURATION
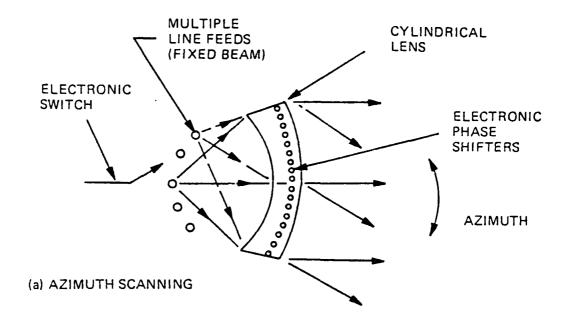
The antenna configuration selected for fabrication consists of the lens and a single line feed. Figure 2-5 shows the basic antenna configuration comprising the cylindrical lens and its on-axis feed. An h_{max}. of 0.52 was selected, corresponding to an $F/D = 0.96$.

The horizontal aperture dimension D was chosen as 40 wavelengths at 5.3GHz, or about 7.4 feet. The vertical length of the line feed Lf is about 35 wavelengths or 6.5 feet, and the lens vertical dimension is 38 wavelenths, or 7 feet.

The lens contains 62 layers of microstrip circuits, each layer containing printed dipoles and interconnecting transmission lines.

2.4 LINE FEED

The horizontal aperture of the line feed must be designed to provide a lens illumination shaped to attain low azimuth sidelobes. Also, the illumination must be very weak beyond the sides of the lens so that the overall antenna sidelobes are not

(a) AZIMUTH SCANNING

(b) ELEVATION SCANNING
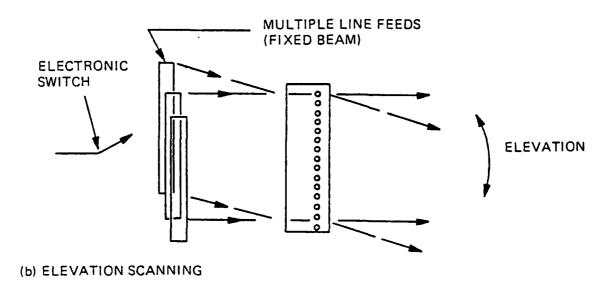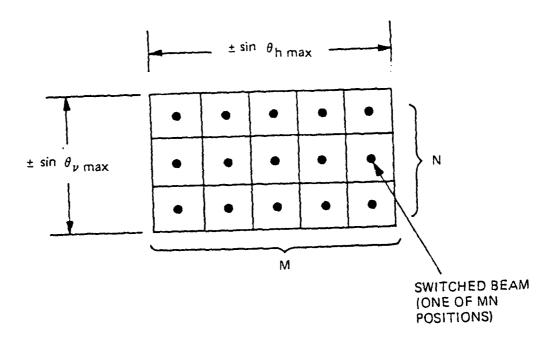
Figure 2-4.   Cylindrical Lens Antenna for Wideband
Wide-Angle Electronic Scanning

2-7

The cylindrical lens antenna has the capability for providing a wideband beam at the center of each sub-region. Each beam in a different azimuth direction requires a line feed that is appropriately displaced in azimuth, as indicated in figure 2-4(a). Each beam in a different elevation direction requires a line feed having collimated radiation that is steered by fixed time delays to the appropriate elevation angel, as indicated in figure 2-4(b). An electronic switch connects in sequence to each of the M x N line feeds, to provide the coarse steering from one sub-region to another. Electronic phase shifters located in the cylindrical lens provide the fine steering over each sub-region.

Each coarse beam position provides wide signal bandwidth because the lens antenna with multiple line feeds provides true time-delay steering and focusing. The phased array located in the lens uses simple phase shifters for finesteering the beam, but achieves wide signal bandwidth because of the relatively small size of the sub-region compared with the full scan coverage of the antenna.

ANTENNA SCAN COVERAGE:

PHASED-ARRAY COVERAGE:

Figure 2-3. Approach for Wideband Wide-Angle
Electronic Scanning

Figure 2-2.   Scanning With a Cylindrical Lens Antenna

The fourth degree of freedom, namely, the lengths of the interconnecting transmission lines, is used to control the change of azimuth focusing that may occur with the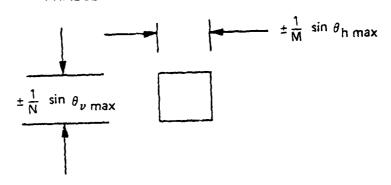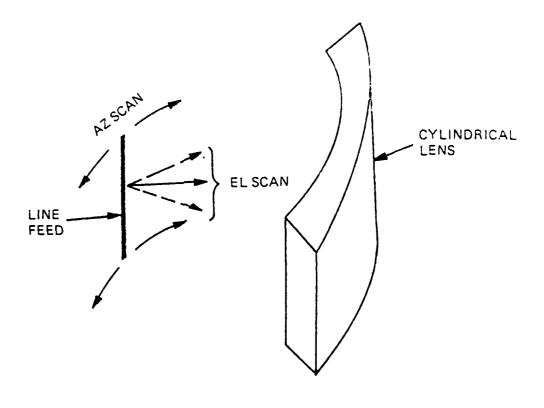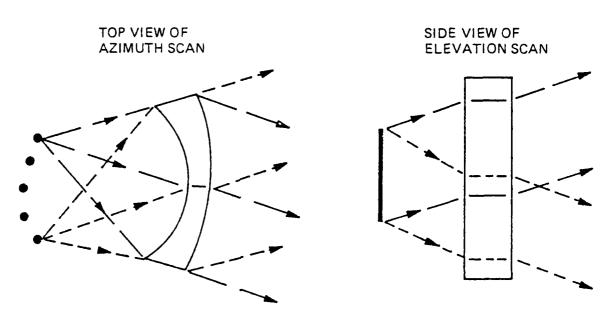 three-dimensional lens when elevation angle is varied. In particular, Rotman and Franchi show that if the lengths of the interconnecting transmission lines are constant throughout the lens, the three points of perfect azimuth focusing are retained independent of elevation angle. Furthermore, at intermediate azimuth angles the azimuth aberration at any elevation angle is no greater than the azimuth aberration of the two-dimensional lens.

The significance of this result is that a cylindrical lens designed in this way can, when combined with an appropriate line-feed system, provide wide-angle scanning of a narrow pencil beam in both azimuth and elevation. For azimuth scanning the line feed is displaced in azimuth, while for elevation scanning the line feed aperture is phase steered. This is illustrated in figure 2-2.

The ability of this constant-line-length cylindrical lens to permit elevation scanning without aberration is analogous to the similar ability of the widely used cylindrical reflector. However, the azimuth-scanning capability of the cylindrical reflector is severely limited by its coma aberration and by the aperture-blocking effect of any centrally-located feed system. The cylindrical lens avoids these limitations.

A phased-array antenna that is electronically scanned can rapidly steer a narrow pencil beam over wide angles. However, if the signal bandwidth (instantaneous bandwidth) is not large, then a phased-array antenna can degrade the signal when the array scans over wide angles. One approach to this problem employs variable time-delay devices in the antenna, but these have some disadvantages. An alternate approach (refs 1, 2, 3, 4) employs the cylindrical-lens antenna as the feeding system for a standard electronically scanned phased array.

Suppose that the scan coverage of an antenna is $\pm \sin \theta_h$ horizontally and $\pm \sin \theta_v$ vertically. This coverage can be divided into M by N equal-size sub-regions, so that each sub-region covers only $\pm (1/M) \sin \theta_h$ by $\pm (1/N) \sin \theta_v$ as indicated in figure 2-3. If the feeding system for the phased-array antenna can provide a wideband beam that can be electronically switched from the center of one-sub-region to another, then the phased array needs to scan over only the relatively small sub-region rather than over the full coverage of the antenna. This will permit a much wider signal bandwidth to be handled without substantial degradation of the signal.

2-3

2.6 ELEVATION PATTERNS

The elevation pattern of the cylindrical lens antenna is similar to the elevation pattern of the line feed. Therefore the line feed should be designed to radiate a low-sidelobe, far-field elevation pattern. However, an additional factor affecting the antenna elevation pattern is the diffraction caused by the top and bottom edge of the cylindrical lens.

This diffraction effect could be made small by having a lens vertical dimension much larger than the line-feed vertical dimension. The diffraction effect can also be reduced by using a well-tapered vertical excitation of the line feed. We have chosen the modified sin u/u distribution (refs 8, 9) for the line feed because it is well tapered and can provide low sidelobes. The lens was made a small amount larger than the line feed.

The nominal vertical-excitation amplitude of the line feed was chosen for a nominal first-sidelobe level of -45 dB. The vertical excitation is provided by a microstrip power-divider network (discussed in a later section) and a set of interconnecting cables. The cable lengths were chosen so as to provide constant path length to the elements of the line feed for radiation at 0° elevation. A second set of cables will provide a time-delay-steered elevation angle of radiation.

The line-feed array was previously shown in figure 2-6. There are 58 elements along the 35 wavelength line feed, giving a vertical spacing between elements of about 0.6 wavelengths. The computed elevation pattern of this line feed array is shown in figure 2-11 for a beam at 0° elevation.

Ref 8 - H. Jasik, "Antenna Engineering Handbook", McGraw-Hill, pp. 2.27-2.28; 1961.

Ref 9 - R. C. Hansen, "Microwave Scanning Antennas", Academic Press, Vol. 1, pp. 58-60; 1964.

In order to determine the effect of lens diffraction on the elevation pattern sidelobes, a pattern computation was performed that included the truncation by the lens of the near-field radiation of the line feed. Figure 2-12 shows the line feed and the inner surface of the lens. Also indicated are rays emanating from the top and bottom of the line feed; the intersection of these rays with the inner surface of the lens is shown by lines drawn across the inner surface. For this case of no elevation scan, these "ray illumination boundary" lines are straight. Of course, the actual illumination of the lens surface is given by the near-field radiation of the line feed, which is only approximated by the ray viewpoint.

Figure 2-13 shows the antenna elevation pattern computed from the actual lens illumination, ie, the near field of the line feed, when the vertical dimension of the lens is 37 wavelengths. Comparison with figure 2-11 shows that the sidelobes are slightly affected by the lens truncation action.
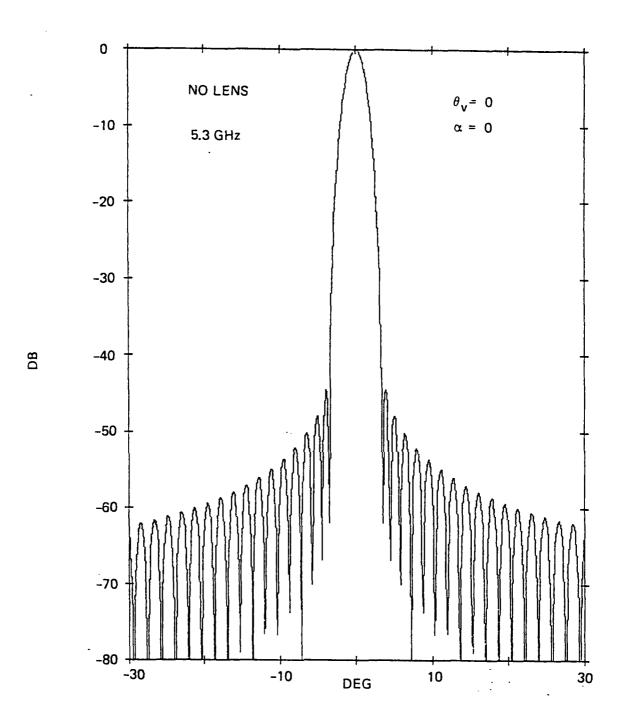
Figure 2-11. Elevation Pattern of Line Feed, $\theta_V = 0$
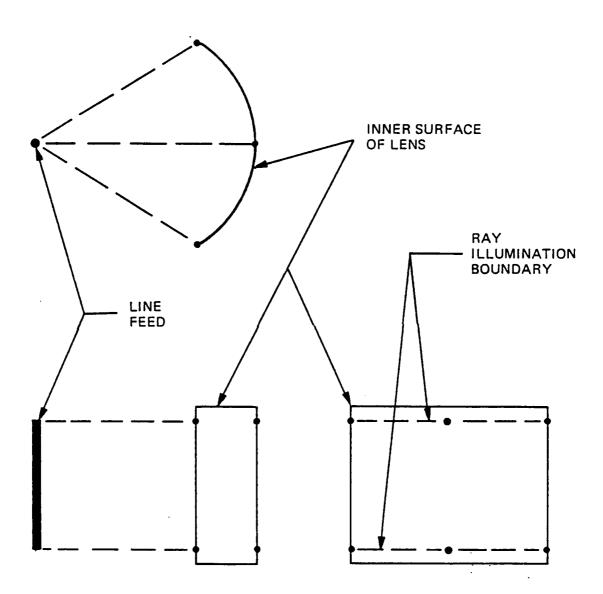
$\theta_v = 0$ $\alpha = 0$
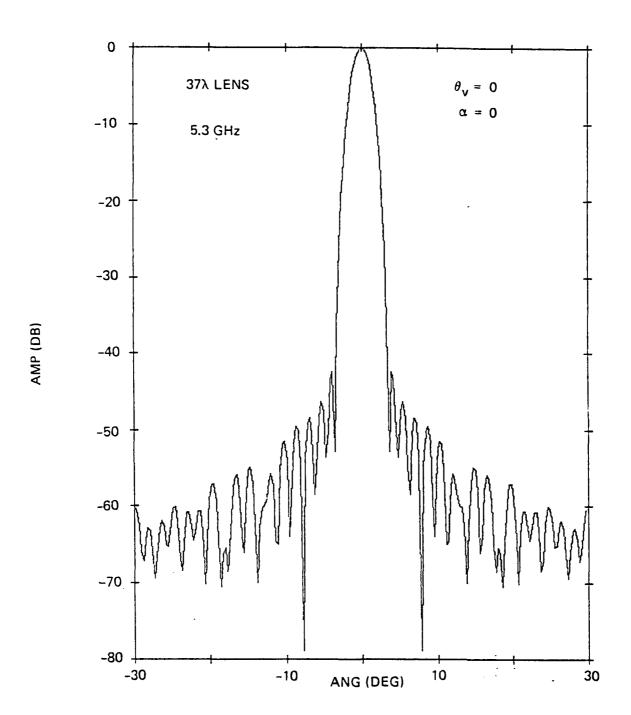

Figure 2-12.   Ray Illumination of Lens, $\theta_v = 0$

Figure 2=13.   Elevation Pattern of Lens Antennna,
$\theta_v = 0$, 37λ Lens

SECTION III

DESCRIPTION OF ANTENNA

3.1. LENS MICROSTRIP LAYERS

The wideband lens array consists of two principal components; the line feed and the lens. Both are constructed of lightweight microstrip transmission lines and components.

The lens layers have been designed on the Calma GDS II graphics system. Associated photo-artworks for etching were fabricated on a Gerber photo plotter from Calma generated data tapes. A typical layer is shown in Figure 3-1.

Through the versatility of the Calma system in the layout design, it was possible to fabricate one-half of a lens layer on a standard 24" by 36" panel. Figure 3.2 shows how the layer was broken up to realize these dimensions. This layout approach reduced the amount of excess material required to fabricate a layer and, thus, the cost of the lens. In addition, acceptable tolerance values associated with both the photo artwork reproductions and etching process are difficult to attain in fabricating panels longer than 36 inches.

Because the electrical length of the lines in each lens layer is several thousand degrees, the phase of each layer is highly dependent on the dielectric constant of the material each layer is etched on. To compensate for material variations, different linelengths were used on materials with different dielectric constants.

Five different artworks were generated for the lens layer. Each individual artwork contained equal phase lines for the 53 transmission paths. Between artworks, the physical length of each transmission path was adjusted to provide an absolute phase equality between layers manufactured from material with slight dielectric constant variations. Our fiberglass material has been manufactured to a ±.02 dielectric constant and measured to an average value within ±.01.
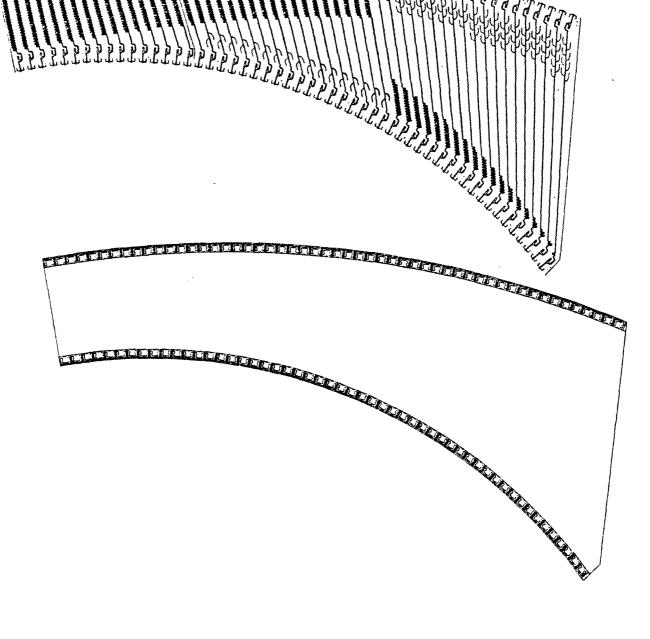
3-1
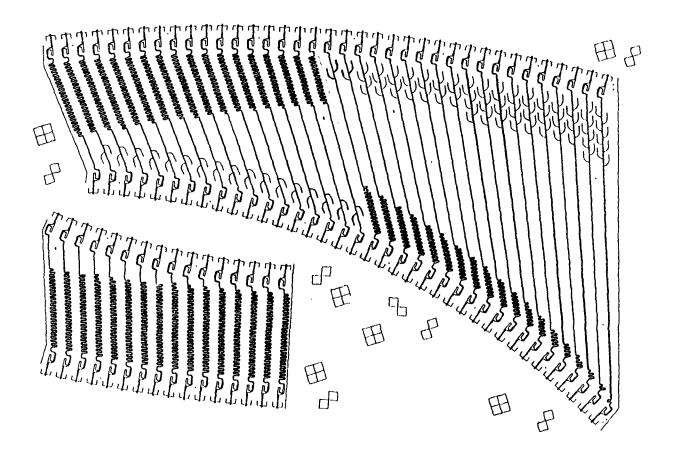
Figure 3-1. Typical Lens Layer

Figure 3-2. Typical Lens Artwork

Dimensional information, for drilling and cutting the lens
sections from the etched panels, was also Calma generated.

3.2 LENS STRUCTURE

Figure 3-3 shows the detailed construction of the lens
layers, each containing 106 printed microstrip lines and
associated radiating elements. Each layer is fabricated in
4 pieces, which are trimmed, drilled and mounted on an
aluminum backing plate. The dipoles project beyond the
metal ground-plane by approximately one-quarter wave. A
vertical aluminum ground-plane, supported by the standoffs
which space the layers of microstrip, is positioned behind
the dipoles. A gap between the dipole feed lines and the
ground plane is maintained to prevent short circuiting of
the feed lines. The ground-plane controls the radiation
pattern of the dipole and also provides limited shielding
for the microstrip transmission lines.

A photo of the lens, without radomes, is in Figure 3-4. It
consists of 62 layers of printed microstrip. The lens
structure is supported by a half-inch thick aluminum plate
at the base, and two channeled vertical side-wall
structures. The base-plate also serves to position the lens
on the antenna support structure (figure 3-5) which is used
to align and focus the lens line-feed assembly. Every ninth
lens layer, the microstrip aluminum backing plates are
attached to the vertical wall structures. The lens antenna
is offset approximately one foot from the base-plate to
eliminate ground effects.

The complete lens structure, assembled with radomes to
weather-protect the microstrip layers, is presented in the
photos of Figures 3-6 and 3-7. The radome material and
construction is essentially invisible to the lens. A teflon
material was selected for its durability and good electrical
characteristics. The radome panels are joined with a thin
teflon tape which introduces negligible transmission phase
variation in the areas used. As depicted in the photos, the
radome material easily conforms to the inner and outer lens
contours.

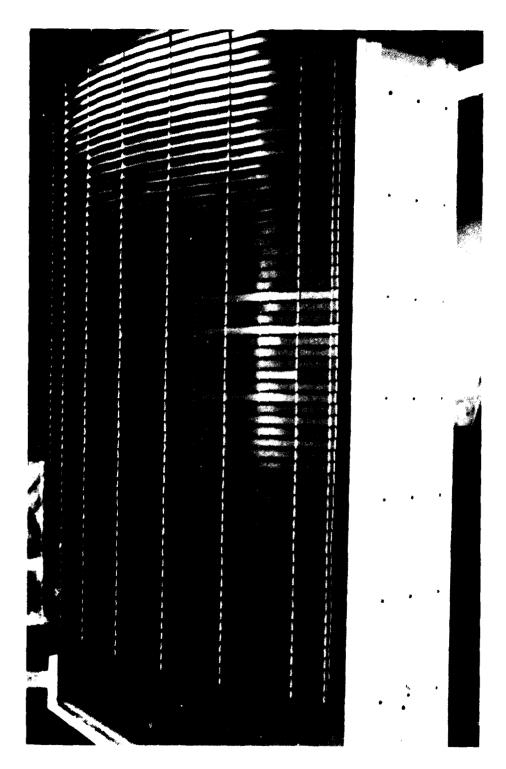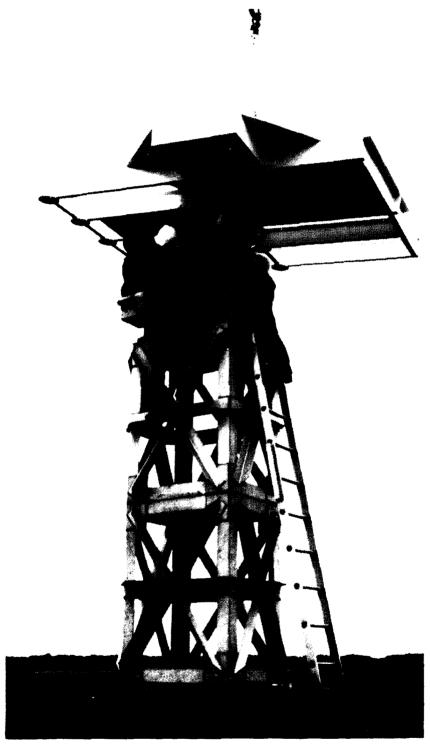Figure 3-3. Detailed Lens Layer Construction

Figure 3-4. Lens Without Protective Radomes

Figure 3-5.   Antenna Support Structure

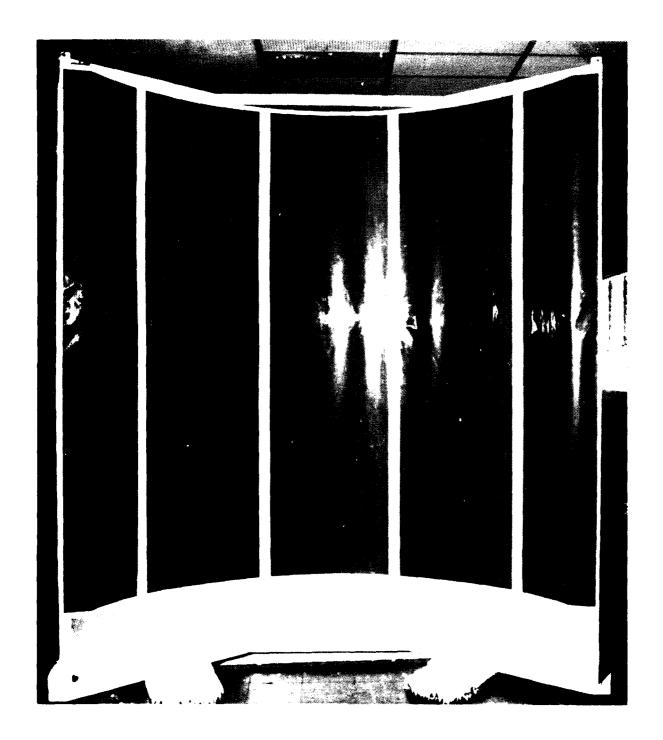Figure 3-6. Front View, Lens with Radome.

Figure 3-7. Rear View Lens with Radome

LINE FEED LOCATIONS
FOR AZIMUTH SCAN

LENS
LOCATION

0⁰   15⁰   30⁰   45⁰
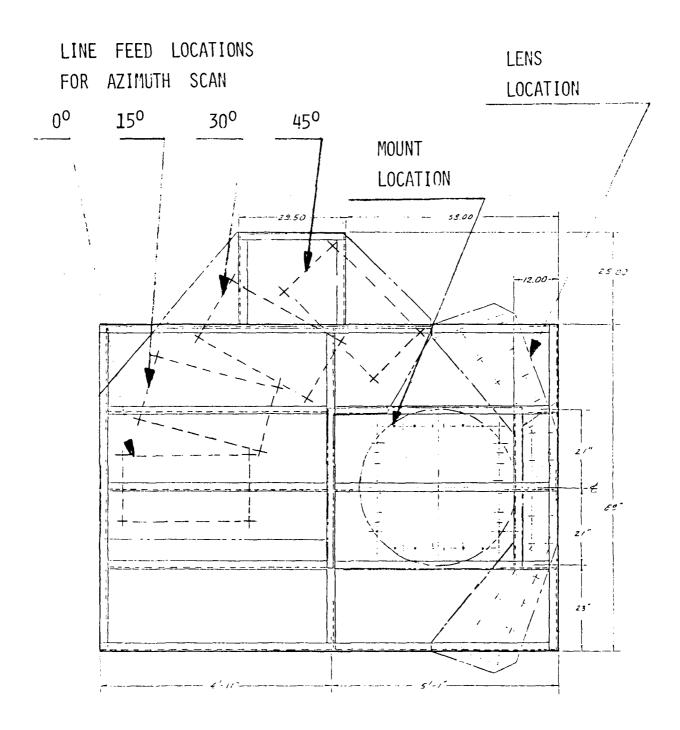
MOUNT
LOCATION

Figure 3-16.   Support Structure Layout

3.6 ANTENNA SUPPORT STRUCTURE

The antenna support structure is designed to align and test the feed in four azimut scan locations, namely 0°, 15°, 30°, and 45°. The feed structure and associated plates interface at each scan location through four alignment holes on the antenna support structure. A layout of the support structure and assembly locations for the lens at various feed positions is in Figure 3-16. Also indicated on the layout is a plate-interface for aligning and holding the structure to our antenna mount during testing.

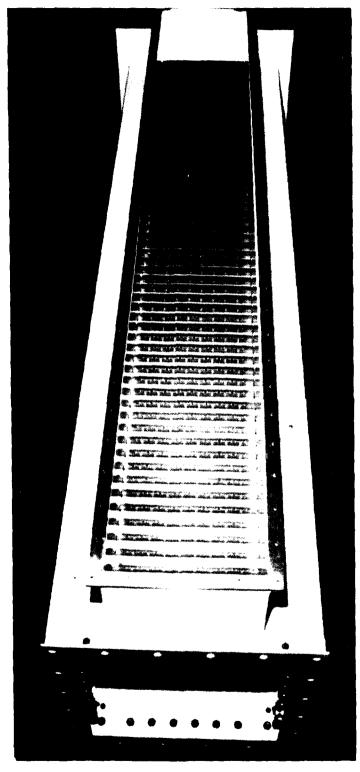Figure 3-15.   Line-Feed And Structure
With Protective Radome

Figure 3-14.   Line-Feed And Housing Structure
                Without Radome

3.5 LINE FEED STRUCTURE

The radiating layers and elevation power divider are
enclosed in a sheet metal cabinet with a thin radome on the
front, to protect the microstrip from weather. Figures 3-14
and 3-15 are photos of the final structure, with and without
the radome.

The line feed assembly is positioned on the antenna support
structure via a base assembly which enables adjustment of
the feed position. The feed structure sits directly on an
offset plate which has been designed to compensate for the
change in location of the feed phase center. Next, a spacer
is assembled to vertically offset the feed to the same
position as the assembled lens. The spacer sits upon two
adjustable sheet-metal plates. The first plate provides an
azimuth tilting capability to optimize the lens
illumination. The second plate allows fine adjustments to
be made in focusing the feed relative to the lens along a
straight line directed at the lens center for each feed
focal position.

A larger spacer has also been designed for the feed
structure. This spacer is used during elevation scanning.
Cables are placed in the feed elevation network to scan the
elevation beam down 15°. The larger offset spacer is
utilized to focus this scanned beam at the lens center,
without increasing diffraction effects significantly from
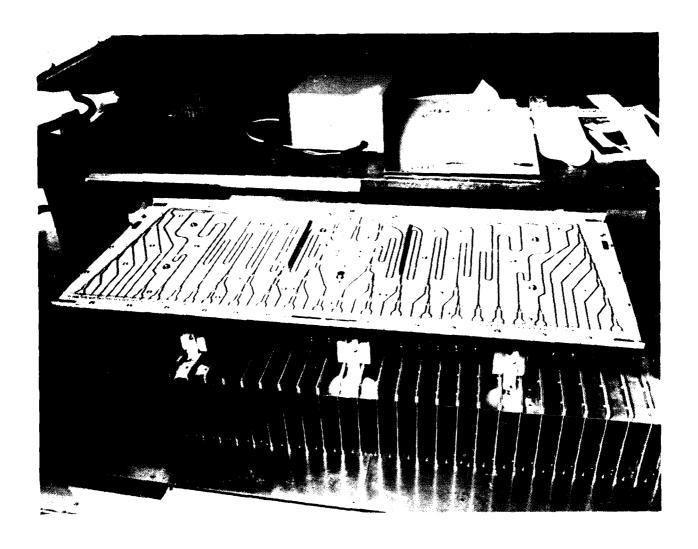the unscanned case.

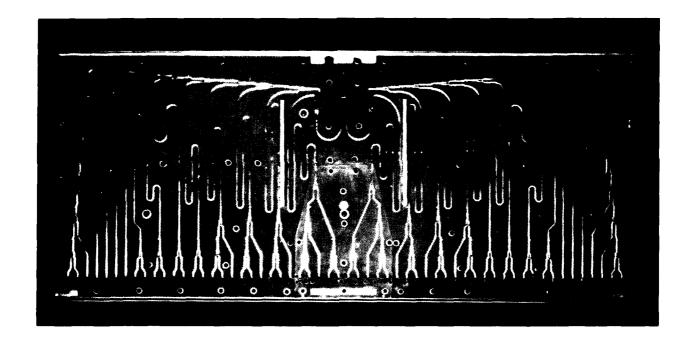Figure 3-13. Assembled Line-Feed Unit

Figure 3-12.   Line-Feed Elevation Power Divider

3.4 LINE FEED ELEVATION POWER DIVIDER

The line feed elevation power divider (Figure 3-12) provides the vertical illumination for the line feed layers. Connectors at the network outputs interface it to the corresponding azimuth layers through semi-ridged cable. Each cable was phase-trimmed to provide equal phase lengths from the elevation input to the cable output over the 5.0 to 5.6 GHz band.

The divider is fabricated on one microstrip board. A sheet-metal backing supports the microstrip and connectors. The fully assembled unit is located mid-way vertically behind the stacked-azimuth layers. The power divider is structurally supported through horizontal stand-offs which attach the power divider to the bent-sheetmetal supports in the column. The assembled layers, interconnecting cables, and elevation power divider are shown in Figure 3-13.
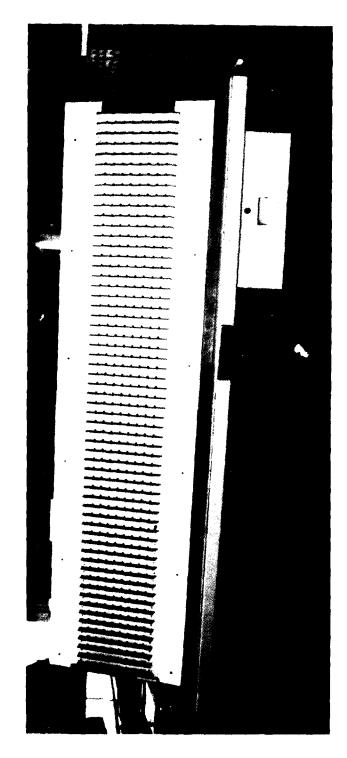
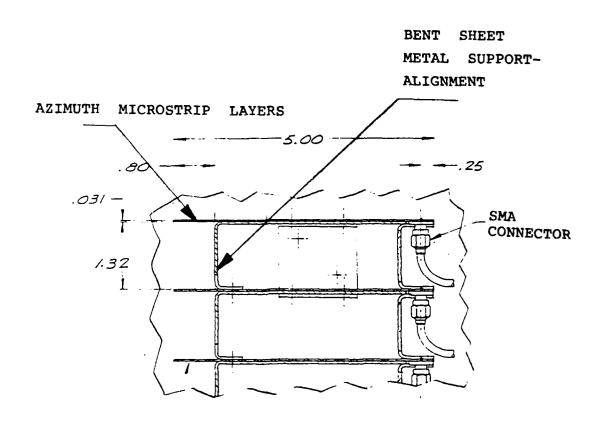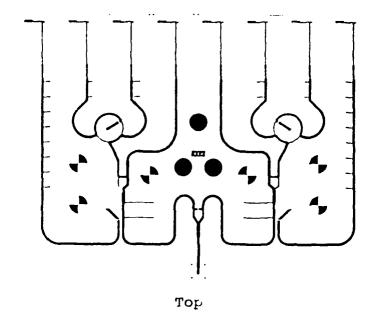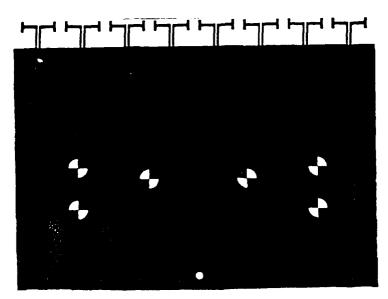Figure 3-11. Lined-Feed Printed Layers

Figure 3-10. Microstrip Layer Construction
For Antenna Feed

Top

Bottom

Figure 3-9. Feed Layer Design

3.3 LINE FEED MICROSTRIP LAYERS

The line feed consists of 58 identical microstrip layers.
The layer design is shown in Figure 3-9. It contains a
horizontal row of 8 dipoles excited by a microstrip power
divider. The resulting current distribution across the
dipole row provides the azimuth feed pattern needed for low
antenna azimuth sidelobes.

Drill holes are located within the layer to provide points
for aligning the layers during assembly of the line feed.
The layers are stacked, aligned and supported by a bent
sheetmetal structure whose design also provides a ground-
backing for the printed dipoles. Figures 3-10 and 3-11 show
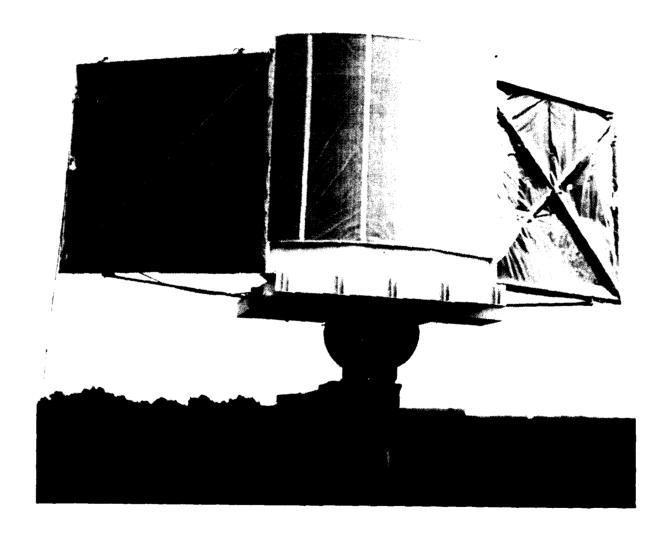the microstrip feed layer construction.

Figure 3-8. Lens Assembly With Absorber Panels

A solution to eliminate unwanted feed radiation spillover is
to provide absorber panels beyond the lens structure. Upon
measurements of the radiation patterns of the final feed
design, the absorber requirement was confirmed necessary.
Absorber panels were constructed and attached to the lens
structure's vertical walls. The interface was accomplished
with a hinge design to allow for adjustment of the panel
angles. The photo in Figure 3-8 shows the absorber panels
on the lens structure. The panels provide 30 dB attenuation
at normal incidence for our frequency band. They have been
made eight feet wide by 8 feet high to sufficiently cover
the spillover sectors.

Each absorber panel is constructed with 16 two foot by two
foot absorber sections glued to a plywood support and
reinforced with an aluminum angle structure. The hinges are
attached to the aluminum angle structure, and mating hinges
are located on the vertical lens walls. A slide tube
support has been designed which connects the absorber panel
to the lens support structure. It is used to adjust and
maintain the desired absorber position for various feed
locations. The assembly is covered with plastic to keep the
absorber dry.

SECTION IV

BREADBOARD DESIGNS

4.1 LENS BENT DIPOLES

To obtain low-sidelobe azimuth patterns when employing
electronic phase shifters for beam scanning required a well-
matched array element in both frequency and scan domains.
This is because multiple reflections create discrete, high
sidelobes. The bent dipole was developed to provide such an
element for the array. A dipole feed and matching technique
were selected that double-tuned the bent dipole design. The
breadboard dipole and feed/matching are illustrated in
Figure 4-1. The dipole is fed by a balun. The patch is
used to single-tune the element and the stubs provide the
double-tuning.

A waveguide simulator was designed to provide an array
environment for the breadboard elements during impedance
matching. A realizable waveguide cross section was
chosen. It simulated a near broadside scan angle of 0° E-
Plane and 8° H-Plane. Six breadboard elements are located
in the waveguide cross-section as shown in Figure 4-2. For
the simulator design to operate properly, the waveguide must
propagate only the fundamental TE-10 mode. A smooth
transition, from a standard waveguide operating in the TE-10
mode to the larger cross-section required for the simulator,
was built to obtain the proper mode propagation. The
transition built (Figure 4-3) is over seven feet long. The
gradual taper was chosen to avoid higher mode propagations
and to minimize phase curvature of the incident wave on the
breadboard elements. Also sh wn in the figure are the
breadboard elements mounted in a support structure that
mates with the transition. In addition, the photograph
displays a short circuit plate which provided a reference
during impedance matching. The six elements were terminated
in their design impedance and adjusted to provide the lowest
reflection in the 5.0 to 5.6 GHz band. Slotted line
measurements were used at the input of the taper to measure
the element reflections. The resulting impedance loci of
the matched-breadboard elements is given in Figure 4-4.

PATCH

DOUBLE TUNING STUBS

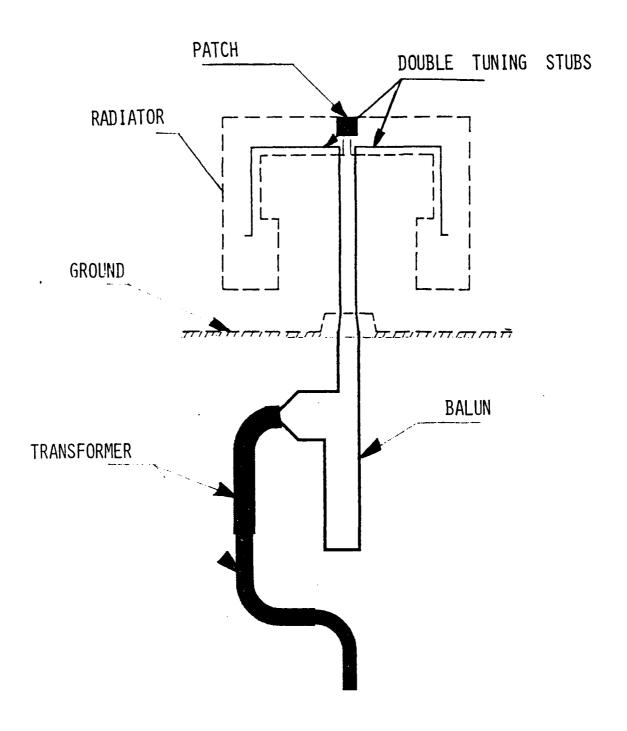RADIATOR
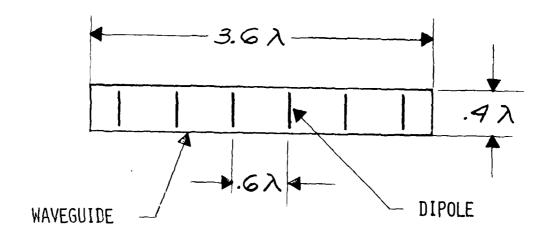
GROUND

BALUN

TRANSFORMER

Figure 4-1.   Bent Dipole Design
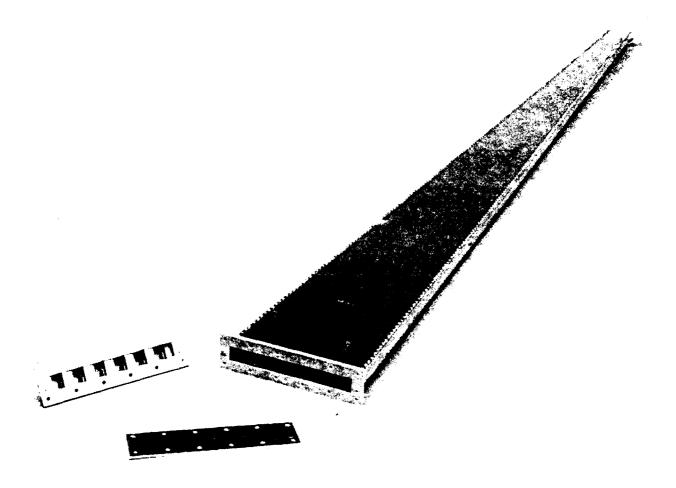
Figure 4-2.   Simulator Array Cross-Section

Figure 4-3. Simulator Transition, Dipole Support
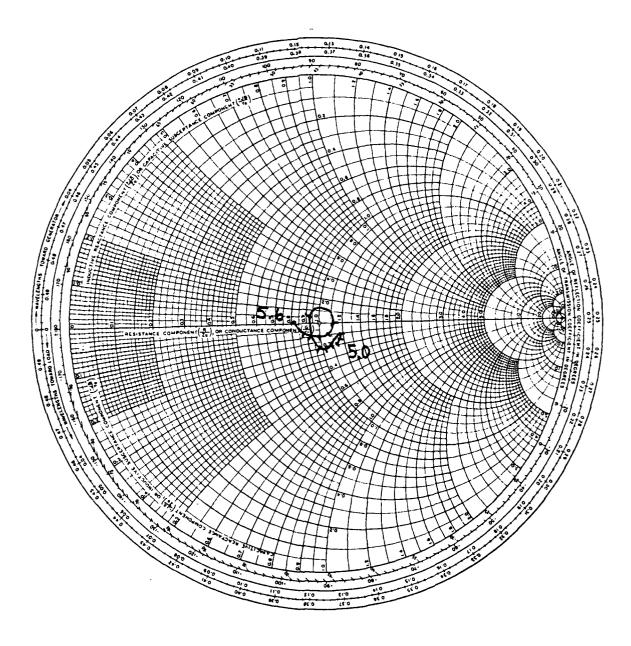Structure, and Short-Circuit Reference
Plate

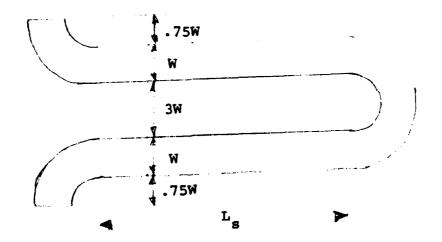Figure 4-4.   Impedance Locus of Matched
Breadboard Lens Array Element

4.2 LENS MEANDERING LINES

In designing the microstrip layers for the lens, meandering
lines were used to achieve the equal line-length connections
between the dipoles on the inner and outer lens contours.
Meandering the lines served two purposes. First, it
simplified the development of the lens layout. Secondly, it
kept the microstrip layers within realizable dimensions for
manufacturing.

A direct layout approach for interconnecting elements
allowed for .4 of available design space. The meandering
line impedance was chosen to provide a reasonable line width
for the layout. To minimize reflections caused by bending
of the meandering lines, it was necessary to provide
quarter-wave spacing between 90° bends. A section of the
line is shown in Figure 4-5.

Breadboard lines were evaluated for successive numbers of
meandering bends. Each was tested for VSWR performance,
transmission amplitude and transmission phase. A typical
bend was characterized in terms of mid-band transmission
phase, and dispersion deviation from an equivalent straight
microstrip line. The lens-layer was then developed using
these measured characteristics. The basic design is shown
in Figure 4-6. Note the number of meandering lines
successively decreases out to the lens edge. The number of
dispersive stubs increase as the number of meandering lines
decrease. Their purpose is to provide the same dispersion
as the straight line, thus equalizing the insertion phase of
all lines over the operating band.

W = .0415 INCH

LS = .230 INCH

THEOR. PHASE = 180^0 AT 5.3 GHz

ACTUAL PHASE = 169.67^0

PHASE FUNCTION = 169.67 + 442.5 (L-.23)

# W RAPS	CALC	MEAS
1	169.67	169.51
2	338.96	339.34
5	848.2	848.4
18	3563.1	3563.1

Figure 4-5. Meandering Line Section

4-7

DISPERSIVE STUBS

MEANDERING
LINES

DIPOLE FEED-TUNING
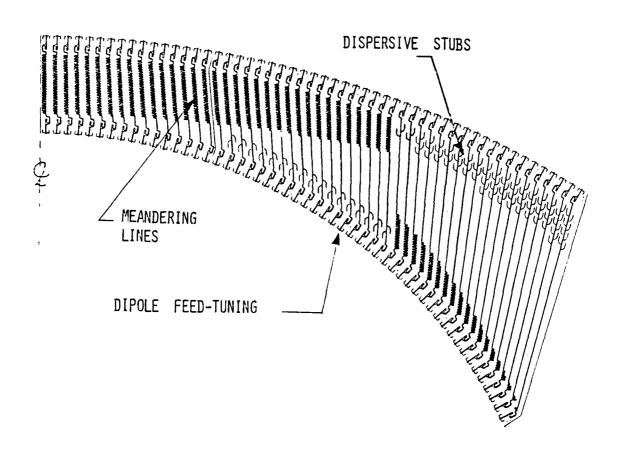
Figure 4-6.   Basic Lens Layer Design

4-8

4.3 LENS LAYER

Utilizing the phase and dispersion characteristics of the
measured breadboard meandering lines, an entire half-lens
layer was designed on the Calma system, photo-plotted and
fabricated. The dipoles on this test piece were replaced
with impedance transformer sections and 50 ohm connectors to
simplify testing. A section of the layout is shown in
Figure 4-7.

Each line was measured for relative transmission phase over
the 5.0 to 5.6 GHz band. Corrections were then made to the
basic Calma layout for the final layer design.

4.4 LINE FEED DIPOLE

A simple straight-arm dipole design was adequate for use in
the line feed since wide-angle scanning was not necessary.
The element and feed-tuning layout is shown in Figure 4-8.
The parallel plate construction, sketched in Figure 4-9,
provided a semi-infinite array simulation of the feed for
impedance matching of the elements. Although this simulator
requires a feeding network for the dipoles, the measurement
of impedance of an element at its feed point was quite
simple. Results of the final dipole tuning over the 5.0 to
5.6 GHz band are in Figure 4-10.

4.5 LINE FEED SMALL ARRAY

A small array was built to empiracally optimize the
horizontal excitation of the line feed. The theoretical far
field azimuth pattern needed for generation of low-sidelobe
lens patterns, set the design criteria for the
illumination. This empirical final design includes the
effects of dipole coupling and dipole feed stem coupling in
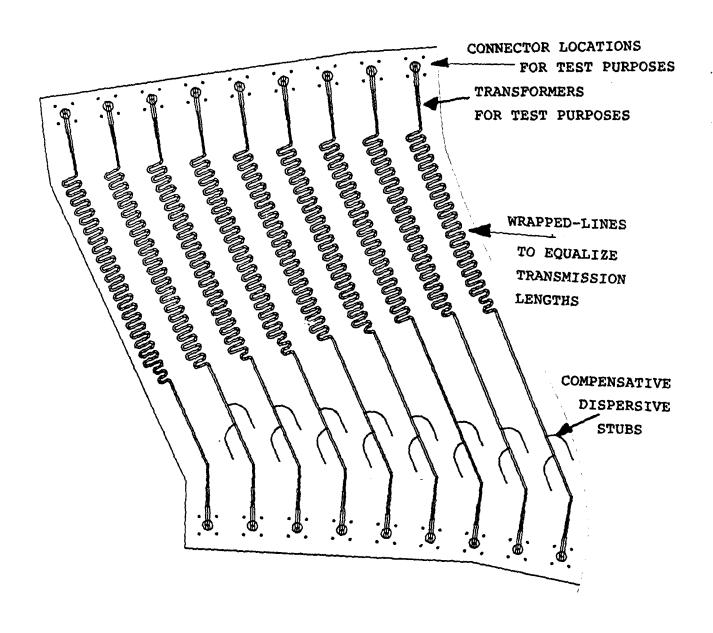finalizing the amplitude and phase settings for the array's
columns.

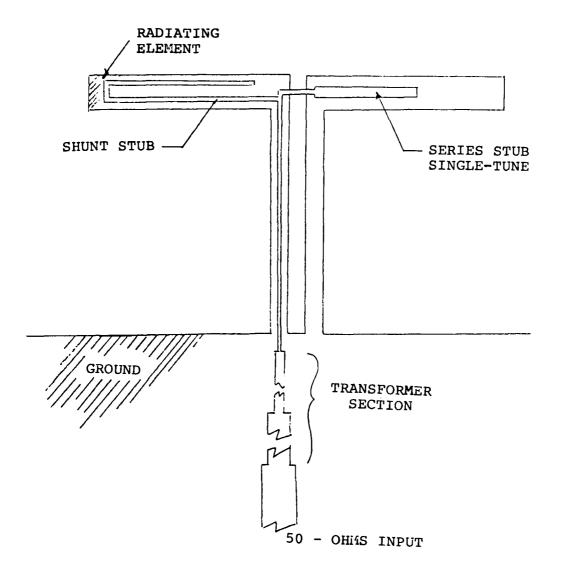Figure 4-7. Breadboard Lens Layer Section

RADIATING
ELEMENT

SHUNT STUB

SERIES STUB
SINGLE-TUNE

GROUND

TRANSFORMER
SECTION

50 - OHMS INPUT

Figure 4-8. Dipole For Feed Array

DIPOLE
GROUND
PLANE

SLOTS FOR
DIPOLE
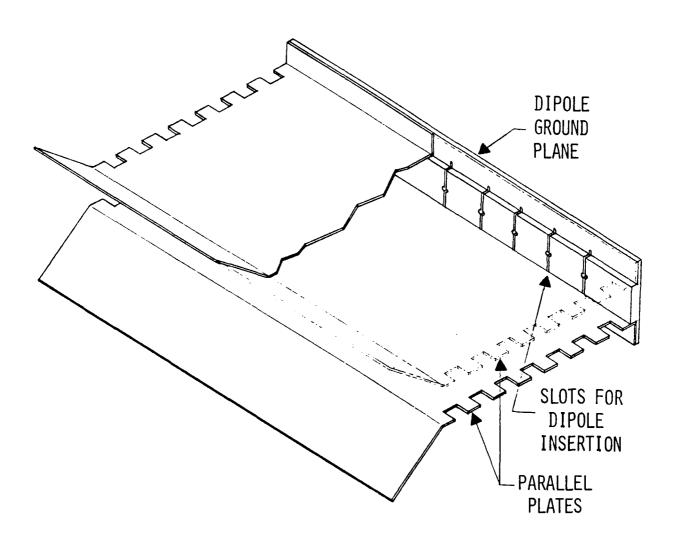INSERTION

PARALLEL
PLATES

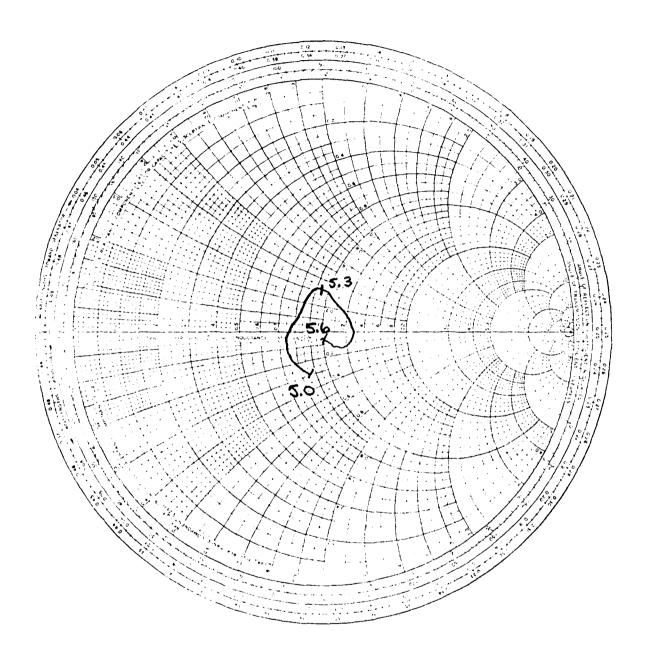Figure 4-9.   Simulator For Matching Line Feed Element

4-12

Figure 4-10. Impedance Locus of Matched Feed Dipole
in Parallel-Plate Simulator

Figure 4-11 is a sketch of the small array and network. The array size was chosen eight elements wide by eight elements high. Those dimensions were selected to match the actual line feed in width, and to be adequately high so that mutual coupling effects are similar to the full height line feed. The eight outputs from each column are combined through eight-way power dividers equal in amplitude and phase. The column outputs are equally combined in symmetrical pairs through two-way power dividers. Each of these four outputs have individual in line attenuators and phase trimmers. The four adjustable outputs are combined through a final four way power divider. Initially, the system was phase-trimmed such that the total transmission phase from the network input to any individual dipole was equal. The theoretical excitation for the array was used as the starting point for setting the amplitude attenuators.

Patterns of the small array were evaluated as fine adjustments in amplitude and phase were made until acceptable azimuth patterns were obtained over the 5.0 to 5.6 frequency band. The relative amplitude and phase setting were then measured for the final feed design. The breadboard small array is shown in figure 4-12.

4.6   LINE FEED AZIMUTH POWER DIVIDER

A number of coupler-types were integrated together to form the Azimuth power divider.The breadboard shown in Figure 4-13 was fabricated, tested and phase trimmed to the output amplitude and phase settings of the breadboard small array. The spacing between the divider outputs was chosen to correspond to the required spacing of the horizontal elements in the line feed. This simplifies integrating the printed-circuit dipoles into the design for the line feed layers.

Results of these measurements are shown in Figures 5-5, 5-6, and 5-7 for frequencies of 5.0, 5.3 and 5.6. As might be expected, the performance is best at 5.3 GHz, the frequency at which the trimming was done. The elevation pattern sidelobes are somewhat worse at the band edges. The peak sidelobes are marginally above the design goal of -28 dB, but exceed them by no more than measurement error. However, it is likely that few sidelobes exceed -28 dB, principally due to variations in phase which could not be trimmed out.

Azimuth patterns of the feed were also measured. Although the patterns could have been evaluated by comparing them to theoretical feed patterns, it would be difficult to define an acceptable variation. Thus we chose to evaluate the patterns by digitizing them and plugging the values into our computer analysis of the complete lens antenna.

Figures 5-8, 9 and 10 show measured azimuth patterns at 5.0, 5.3 and 5.6 GHz. The azimuth pattern was specifically designed to provide a shaped illumination across the lens, and sidelobes below -40 dB at angles beyond those subtended by the lens. The sidelobes were not as low as the theoretical design, but were still well below isotropic and were very good considering that they were achieved by an 8 element array.

Peak levels of -28 dB are shown in the three patterns. Because levels such as these would result in unacceptable sidelobe levels for the entire antenna, absorbing panels will be placed on each side of the lens to absorb feed radiation.
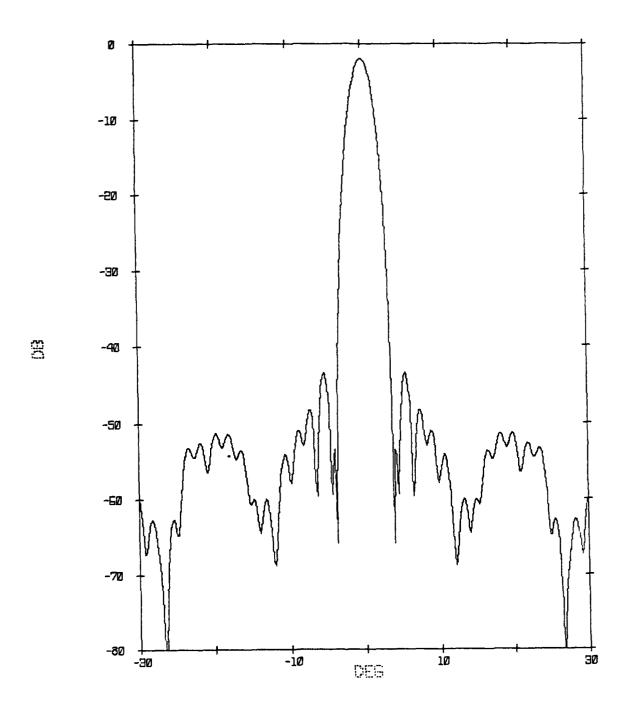
Figure 5-4. Simulated Elevation Feed Pattern From
Measured Elevation Network Outputs

5.2 LINE FEED TESTS

The line feed was tested on the Smithtown antenna range before being installed with the lens. Both azimuth and elevation patterns were measured.

Considerable effort was devoted to achieving low sidelobe elevation patterns. The elevation illumination is determined by the microstrip power divider and its associated cables. Initial measurements of the line feed elevation pattern showed sidelobe levels significantly higher than those calculated from the measured output amplitudes of the microstrip network. Figure 5-4 shows the pattern calculated from the measured outputs, with resulting sidelobes of -37 dB.

Since the combined microstrip network and the semirigid cables (used to connect to the azimuth power divider) had been measured together and phase trimmed, we concluded that the microstrip azimuth power dividers were introducing significant phase errors. Although the azimuth power dividers were etched from material from a single batch of teflon-fiberglass boards to minimize variations in dielectric constant, the variation within the boards was great enough to introduce significant phase variations.

Measuring the phase through the azimuth power dividers represented a significant challenge because the output was not accessible to a network analzer. A coupler was constructed which coupled to the microstrip line near one of the edge dipoles. Despite a weak coupling level (-20 dB), measurements were repeatable to within ± 3 degrees. Using this test setup, the insertion phase of the feed was measured from the network input to the coupler. Based on these phase measurements, the cables were retrimmed.

Elevation patterns of the line feed were mesured on the Smithtown antenna range. The elevation patterns were measured using the elevation axis of the mount. This procedure was adequate because of the relatively high sidelobes (-28 dB) and low range reflections (-40 dB). Thus the sidelobes have a worst-case error of ±2 dB.

UPPER AZIMUTH PATTERNS
TAKEN 0° TO 90° AZ

ELEVATION AT 90°

LOWER AZIMUTH
TABLE

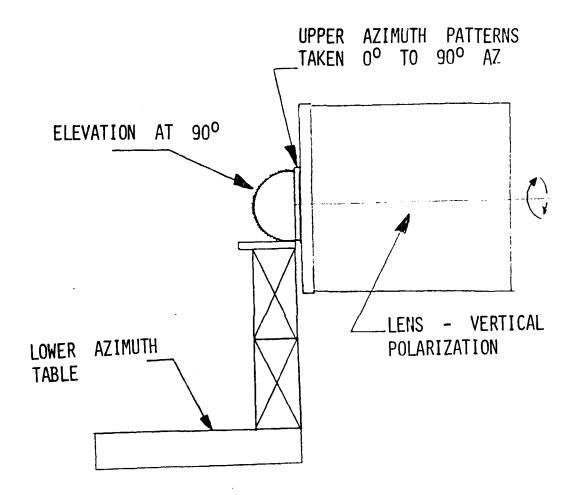LENS - VERTICAL
POLARIZATION

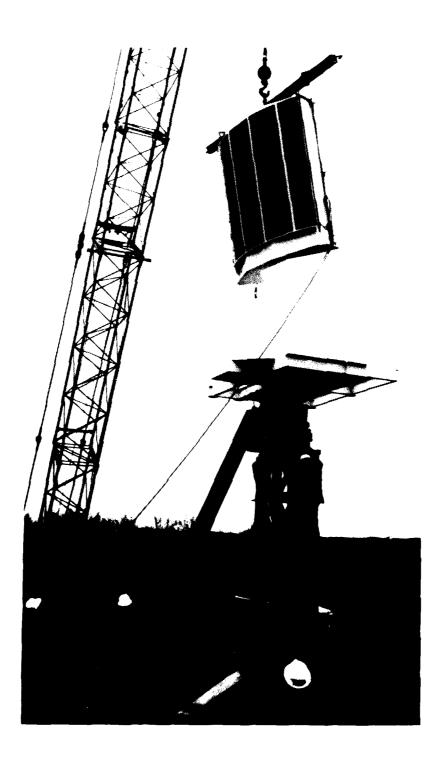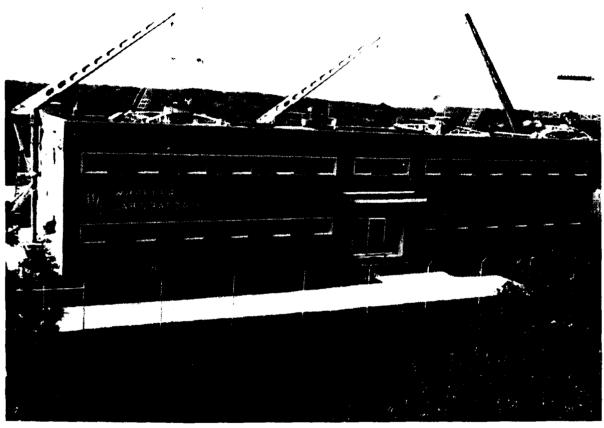Figure 5-3   Improved Antenna Test Setup

Figure 5-2 Antenna Being Positioned in Test Setup

71J1001

Figure 5-1   Antenna Test Facility

directed at or above the horizon. Thus the sidelobes measured are perturbed by a range reflection which is approximately 40 dB below the sidelobe level, resulting in a negligible error.

Pattern measurements were made on Scientific Atlanta equipment, using both manual and automated systems. The measurement equipment has a minimum dynamic range of 60 dB.

SECTION V

PRELIMINARY TESTS AND EVALUATIONS OF ANTENNA

5.1   INTRODUCTION   AND DESCRIPTION TEST SETUP

This section describes the initial testing done on the line
feed, and the combination of the lens and the line feed. It
also describes diagnostic tests and adjustments to the lens
performed prior to final testing.

All pattern testing was performed at Hazeltine's test range
in Smithtown, N.Y. Figure 5-1 shows a photograph of the
test facility. The building is used for assembly and
checkout of antennas before they are installed on the roof
for testing. The top of the building contains seven multi-
axis mounts which are used for antenna testing.

The transmitting source building is located 1000 feet away
across a shallow valley. The source frequency and
polarization are controlled remotely from the main building.

The test setup was configured specifically for the
measurement of low sidelobes. Because a range suitable for
the measurement of sidelobes below -50 dB was required,
special care was taken. The antenna was mounted on a three-
axis positioner, with the upper azimuth and elevation axis
located 10 feet above the lower azimuth positioner, as shown
in Figure 5-2. The positioners are located on the upper
roof of the building, so that there are no nearby reflecting
obstacles in any direction.

The range was probed to measure the level of spurious
reflections. Across a 10 foot square area, the peak
measured amplitude ripple was ± 0.1 dB, corresponding to
reflections of -40 dB. This reflection level is caused by
scattering from the ground and objects which are illuminated
by the source antenna. However, this level of range
reflections, which is at the limit of our measurement
capability, is not adequate to measure antenna sidelobes of
-50 dB. It is adequate for measuring the elevation patterns
of the array.

A more accurate means of measuring very low sidelobe levels
is illustrated in Figure 5-3. Here, the pattern cuts may be
taken so that the main beam of the antenna is always
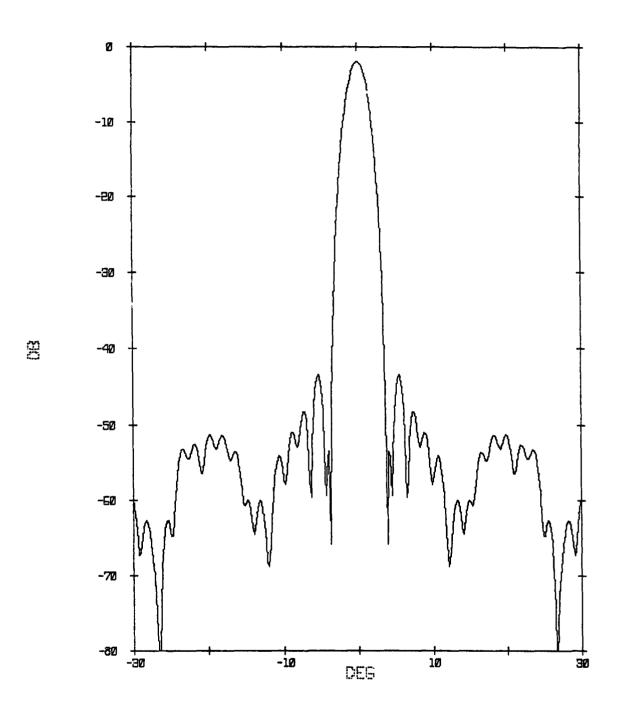
5-1
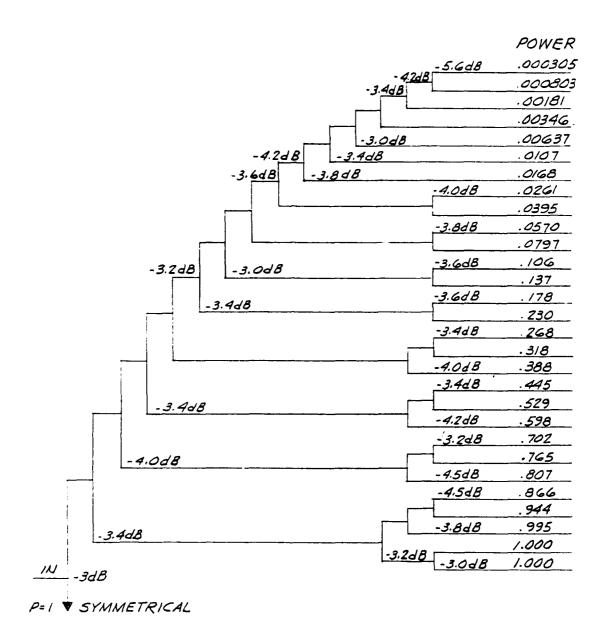
Figure 4-15.   Quantized Coupler Layout

Figure 4-14.   Theoretical Antenna Elevation Pattern
With Quantized Coupler Elevation Network

4-19

4.7 COUPLERS FOR ELEVATION POWER DIVIDER

The layout of the elevation power divider was initially
designed with realizable coupler values for microstrip
fabrication. The coupler values were quantized to nine
values to reduce breadboarding efforts. The calculated
elevation pattern of the lens assuming the quantized coupler
design is given in Figure 4-14. Figure 4-15 is the
corresponding quantized coupler layout for the line feed.
Each individual coupler was breadboarded and matched prior
to fabricating the elevation network.

4-18
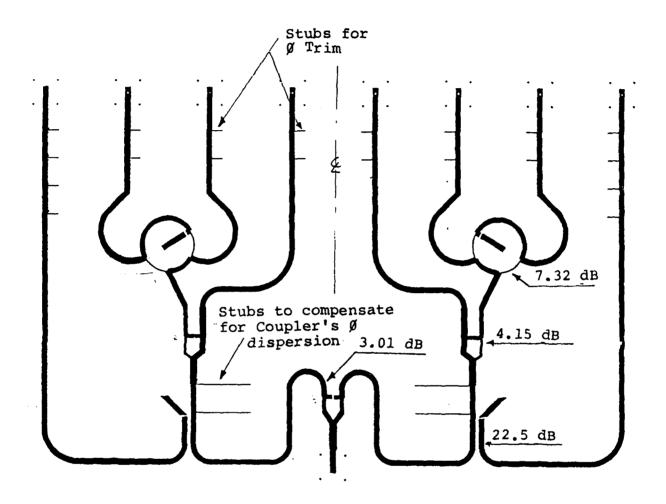
Figure 4-13. Breadboard Azimuth Power Divider
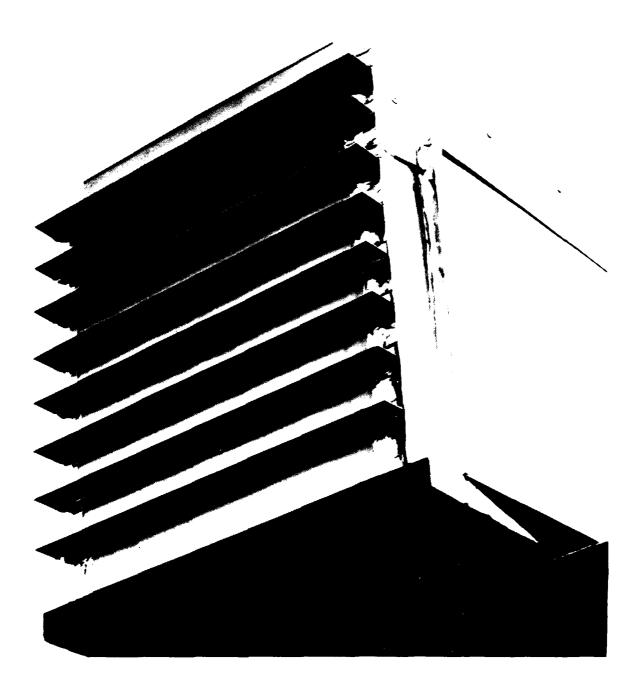
Figure 4-12.   Breadboard Small Array
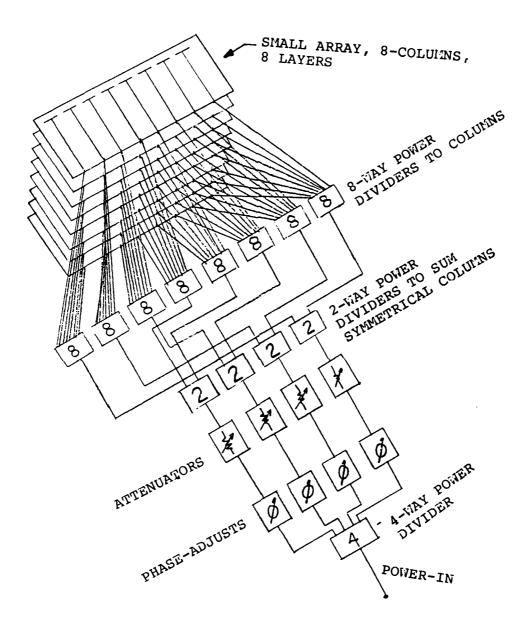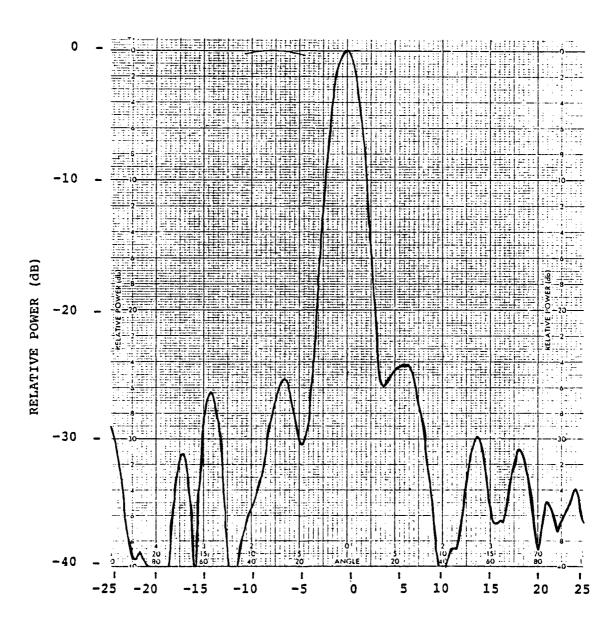
Figure 4-11   Small Array Configuration

Angle (Deg.)

Figure 5-5. Measured Line-Feed Elevation Patterns, 5.0 GHz
For ±30° Sector
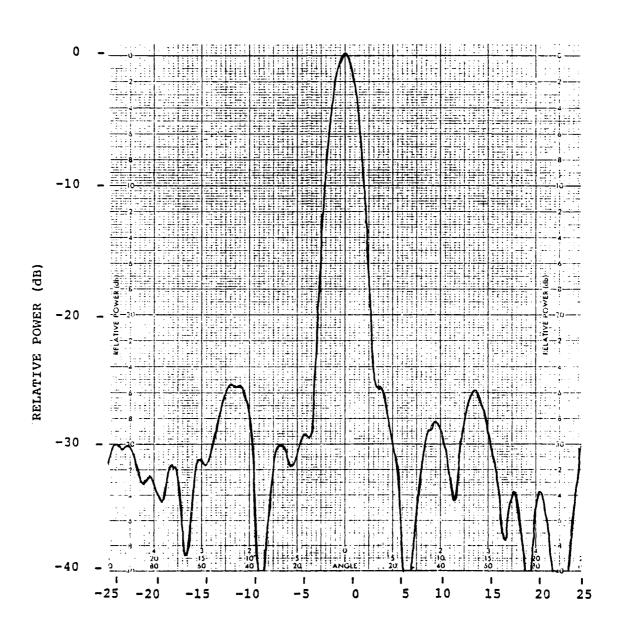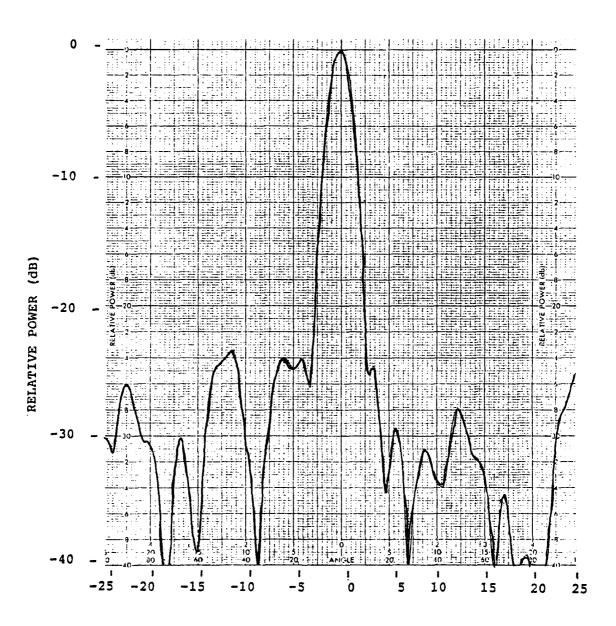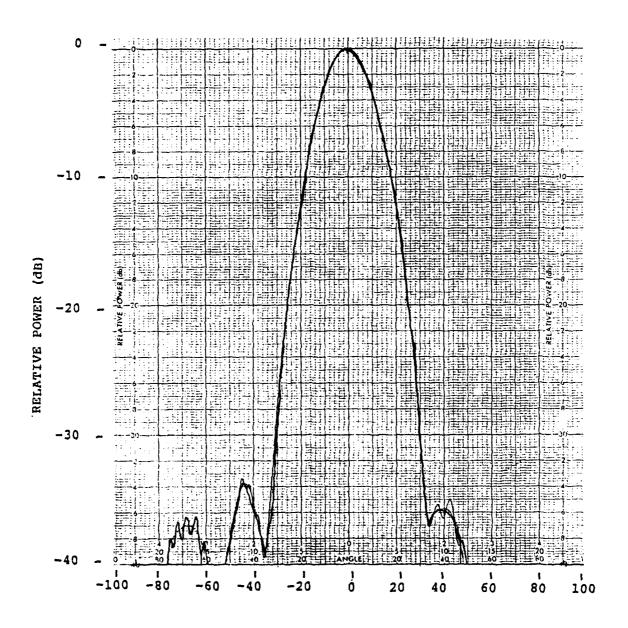
Angle (Deg.)

Figure 5-6.   Measured Line-Feed Elevation Pattern, 5.3 GHz
For ±30° Sector
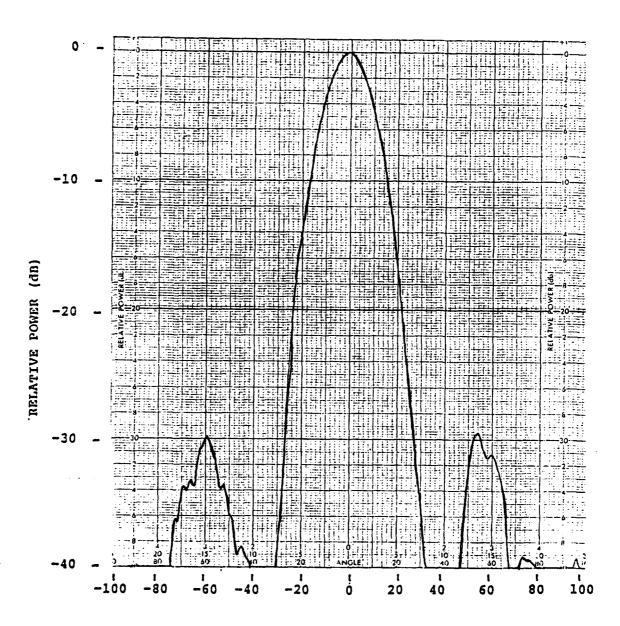
Angle (Deg.)

Figure 5-7.   Measured Line-Feed Elevation Patterns, 5.6 GHz
For ±30° Sector
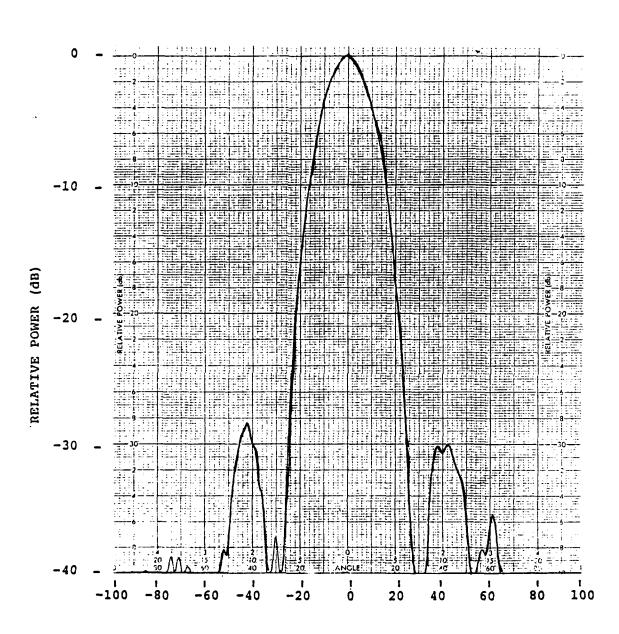
Angle (Deg.)

Figure 5-8.   Measured Line-Feed Azimuth Pattern 5.0, GHz
For ±90° Sector

Angle (Deg.)

Figure 5-9. Measured Line-Feed Azimuth Patterns, 5.3 GHz
For ±90° Sector

Angle (Deg.)

Figure 5-10.   Measured Line-Feed Azimuth Patterns, 5.6 GHz
For ±90° Sector

As described above, the shape of the illumination on the
lens was evaluated by calculation. The calculation assumed
that all the feed radiation outside of the lens is zero, and
that the line feed phase center is that of the theoretical
line feed.

Figure 5-11 shows the lens pattern calculated from the
measured line feed azimuth pattern at 5.0 GHz. Table 5-1
summarizes the sidelobe performance of the calculated
pattern compared to the design goal. The design goal is
achieved or surpassed except for the sidelobes at -50 dB.
This performance was deemed acceptable because these
sidelobe levels were approaching the accuracy of the
measurement. It should be noted that the calculation did
not take into account tolerance errors in the lens, which
may increase the low level sidelobes.

Figures 5-12 and 5-13 show the calculated patterns for 5.3
and 5.6 GHz, respectively. The calculated sidelobe levels
are also summarized in Table 5-1. At these two frequencies,
the calculated patterns satisfy the design goals.

These pattern tests completed the evaluation of the line
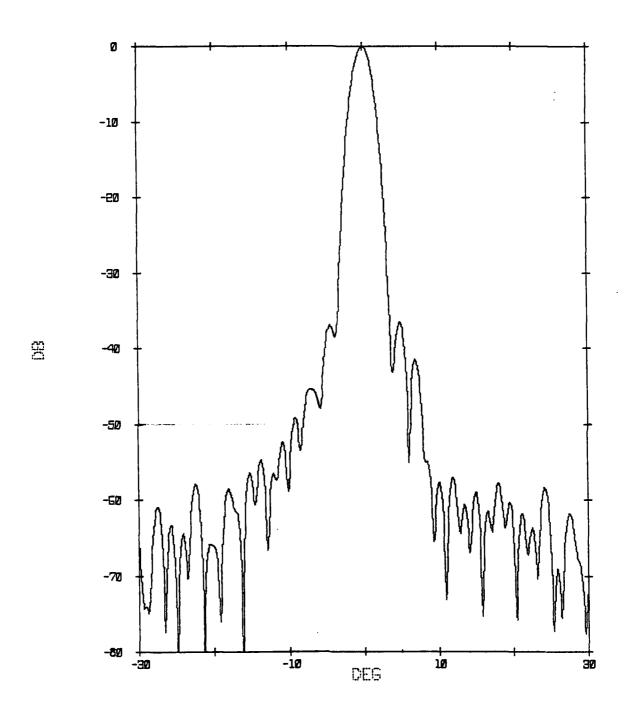feed prior to its integration with the lens.
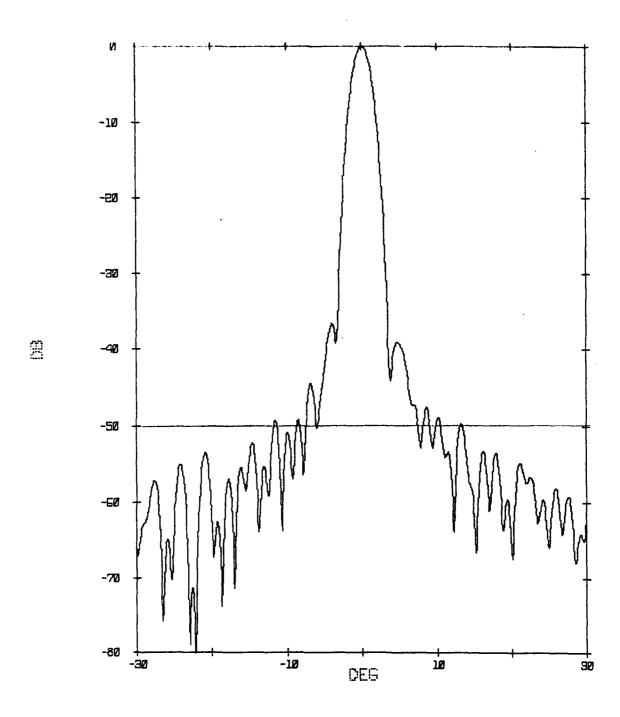
Figure 5-11. Simulated Lens Pattern From Measured Feed
Azimuth Pattern at 5.0 GHz

Figure 5-12.   Simulated Lens Pattern From
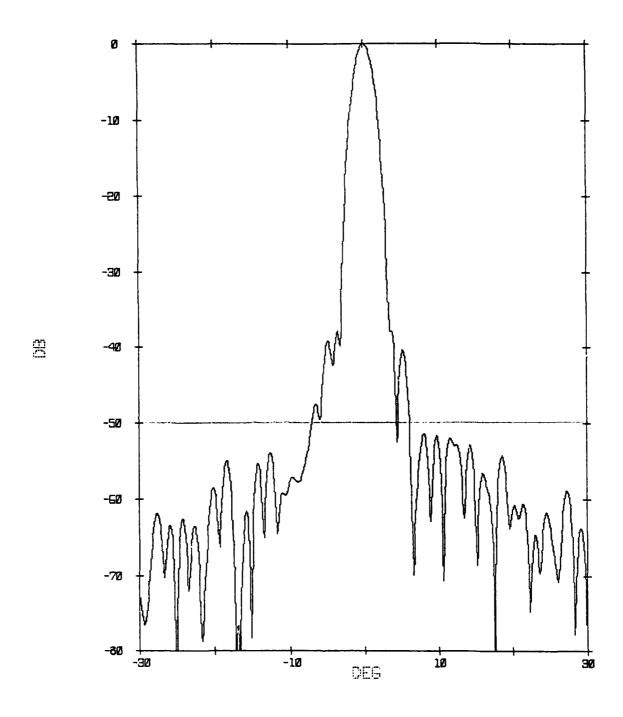Measured Feed Azimuth Pattern
at 5.3 GHz

5-17

Figure 5-13. Simulated Lens Pattern From Measured
Feed Azimuth Pattern at 5.6 GHz

Table 5-1. Calculated Sidelobe Levels

Number of sidelobes between:

	0 to -32 dB	-32 to -37 dB	-32 to -42 dB	-32 to -50 dB
Design Goal	0	2	4	6
Calculated	0	2	4	6
5.0 GHz	0	1	2	7
5.3 GHz	0	1	3	5
5.6 GHz		0	4	5

5.3 MEASURED LENS AZIMUTH PATTERNS AND EVALUATION

Preliminary tests were performed on the antenna at broadside scan. The assembly of the lens, feed and support structure are in Figure 5-14. The absorber structures were not included in these tests, consequently, lens performance was evaluated only within the ±30 degree sector off broadside. Sidelobe levels outside of this region include the effects of feed spillover, which results in significant degradation of the antenna sidelobes.

Results of these tests are shown in the measured antenna azimuth patterns presented in Figures 5-15 through 5-17. The extremely high sidelobe levels could not be reduced significantly during testing with any of the feed-adjustment techniques (i.e. feed tilting and re-focusing) available in the test setup. It was concluded that these results were caused by phase errors in the lens transmission lines. Tests were implemented to confirm that the errors were large enough to result in the measured antenna response.

A dipole coupler was designed to provide a means for measuring transmission phase of the microstrip lines in the lens layers. The coupler developed exhibited excellent electrical characteristics. The amplitude coupling varied between -5 and -7 dB over the 5.0 to 5.6 GHz band. The coupler match was within a 2:1 VSWR and did not significantly degrade the VSWR performance of the lens dipole when in use. Transmission Phase repeatability measurements were able to be made within 5 degrees of accuracy. Two such couplers were built and interfaced with the lens dipoles to measure and compare transmission phase between lines within a lens layer.

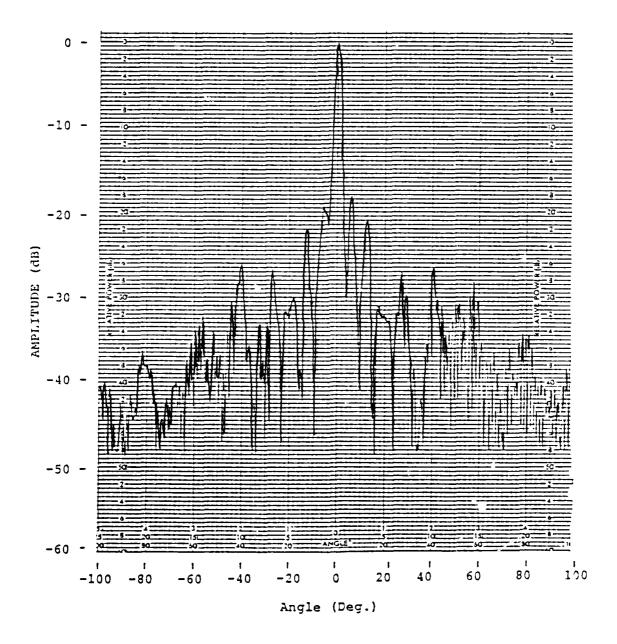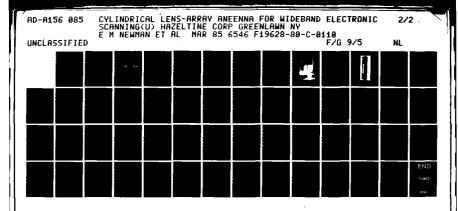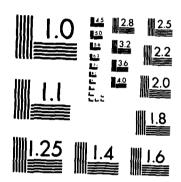Figure 5-14.   Antenna Assembly in Test Setup for
Preliminary Evaluation

Figure 5-15.   Preliminary Measured Antenna
Azimuth Pattern 5.0 GHz

MICROCOPY RESOLUTION TEST CHART
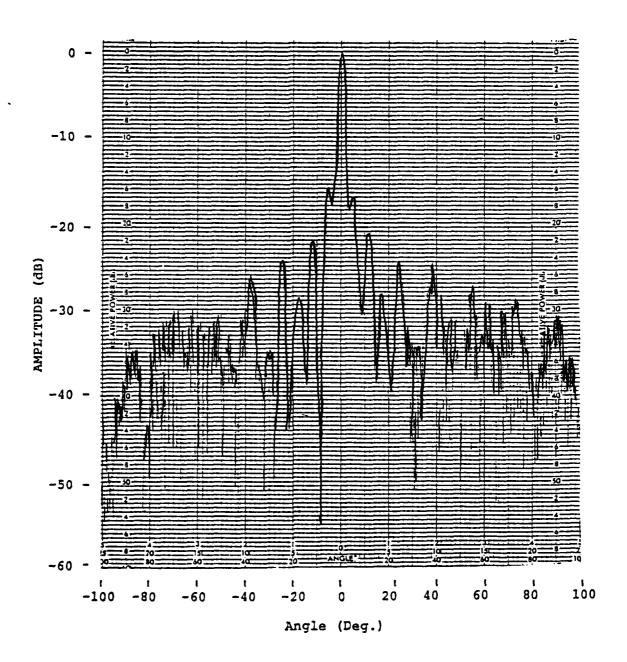NATIONAL BUREAU OF STANDARDS-1963-A

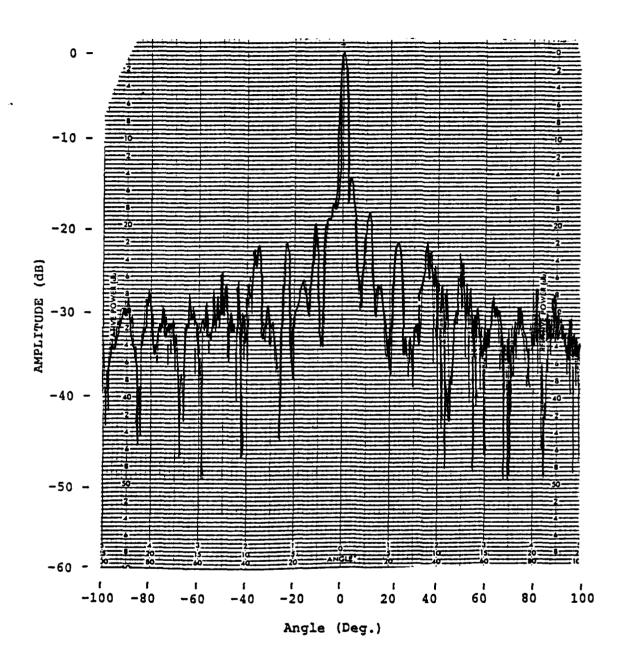Figure 5-16. Preliminary Measured Antenna
Azimuth Pattern 5.3 GHz

Figure 5-17. Preliminary Measured Antenna
Azimuth Pattern 5.6 GHz

A spare microstrip lens-layer was tested. The relative
transmission phase was measured between lines. A computed
lens pattern was generated utilizing these measured phase
errors. Figure 5-18 illustrates the resulting lens pattern.
Comparing the relative sidelobe levels of this pattern to
the preliminary measured azimuth pattern in Figure 5-16
confirms that the lens-layer phases were not held adequately
to obtain the desired antenna performance.

The phase errors result principally from localized
variations in the dielectric constant of each board. It is
possible, although not certain, that a higher quality
microfiberglass Teflon board would minimize the problem.
The following section describes how they were corrected to
improve the antenna.
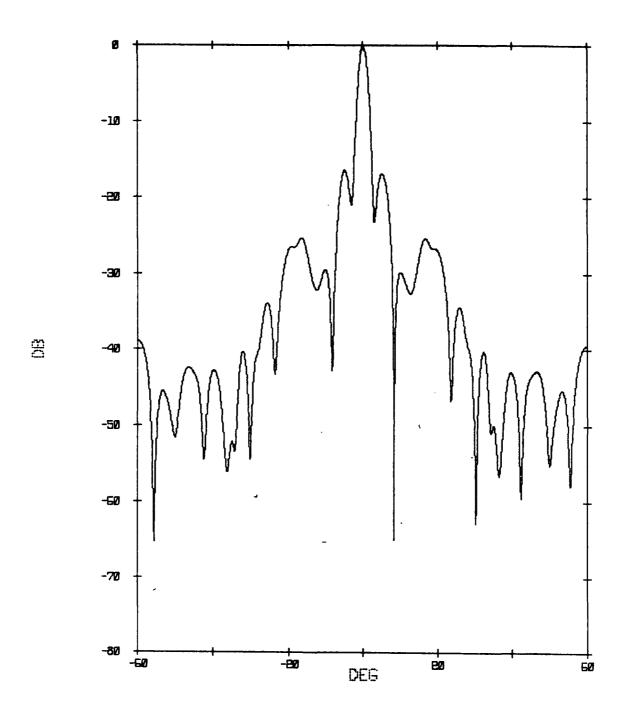
Figure 5-18. Computed Azimuth Pattern of Lens With Measured
Phase Errors of Lens Layer Included

5.4 LENS LINE PHASE CORRECTIONS

The lens layers were measured and phase corrections were inserted by placing a dielectric tape on each line to increase its insertion phase by a desired amount.

The test couplers were used in measuring and identifying the phase variations in the lens layers. The lens radomes were removed, along with the ground strip dir , backings. It was not necessary to fully disassemble ' . lens to perform the phase measurements or corrections

Each lens layer was partially tested for phase variations within the layers transmission lines. Although the variations between all layers was not identical, implementation of an average correction of the lines was possible for layers manufactured from the same artwork. Care was taken to obtain more accurate phase information and not to use average correction values in the lens's central region where the feed illumination is highly concentrated.

A central element was used as a reference in each layer for relative transmission phase measurements. The largest normalized errors were on the order of 80 degrees. Typically, they were less than 60 degrees. Following the identification of the phase variation in a lens layer, each of the lines were adjusted to the electrically longest line apparent in the layer.

Teflon tape was used to trim the lines in the microstrip layers. Lengths of tape were chosen to provide phase corrections in 5 degree increments, to a maximum correction of 60 degrees when placed appropriately on the microstrip lines. The technique was breadboarded to assure the VSWR and transmission amplitude of the microstrip line were not significantly affected by the addition of the tape over a portion of the line.

Figure 5-19 is a list of phase corrections used in one lens layer. Each layer is _not_ identically phase corrected. A correction scheme was developed independently for each layer utilizing measured phase variations in that particular layer.

	LEFT-ELM	RIGHT-ELM
1	-35.	-60.
2	-30.	-60.
3	-45.	-60.
4	-40.	-60.
5	-25.	-60.
6	-30.	-60.
7	-30.	-60.
8	-20.	-55.
9	-15.	-40.
10	-15.	-45.
11	-15.	-45.
12	-25.	-60.
13	-15.	-45.
14	-25.	-40.
15	-15.	-40.
16	-25.	-40.
17	-10.	-15.
18	0.	-20.
19	-20.	-35.
20	-15.	-35.
21	-15.	-30.
22	-25.	-40.
23	-35.	-40.
24	-30.	-40.
25	-25.	-40.
26	-10.	-30.
27	-20.	-35.
28	-20.	-40.
29	-30.	-35.
30	-30.	-35.
31	-30.	-40.
32	-30.	-40.
33	-30.	-45.
34	-10.	-25.
35	-25.	-30.
36	-20.	-30.
37	-10.	-25.
38	-20.	-30.
39	-25.	-30.
40	-25.	-30.
41	-30.	-45.
42	-25.	-30.
43	-15.	-20.
44	-5.	-10.
45	-5.	-10.
46	-5.	-15.
47	-5.	-10.
48	0.	-15.
49	0.	-10.
50	0.	-15.
51	-5.	-20.
52	0.	-10.
53	0.	0.

Figure 5-19.   Phase Corrections of One Lens Layer

SECTION VI

FINAL TEST OF ANTENNA

6.1 SETUP/TEST METHOD

The final antenna tests were made with the absorber structures included in the assembly as shown in Figure 6-1. With the antenna upright, as shown, azimuth patterns were taken over $\pm 90^\circ$, for all azimuth scan positions, relative to the on axis broadside scan angle of 0°. These measurements were made with the source horizontally polarized, using the upper azimuth mount for antenna rotation. Azimuth pattern measurements with the antenna tilted 90° were not made because of the weight of the antenna and structure.

Elevation patterns were also taken with the source vertically polarized. The patterns were taken over a range of $\pm 45^\circ$ for both the 0° and 15° elevation scan case relative to the broadside position. Full pattern measurements were restricted by the weight of the assembly. However, the pattern sector covered is sufficient to demonstrate the scan capability of the system.
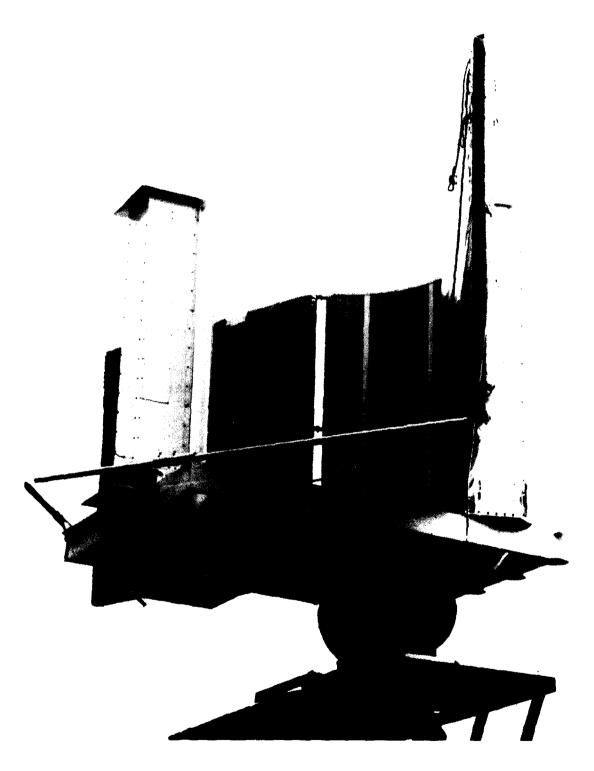
Figure 6-1.   Antenna Assembled for Final Test
at Smithtown Facility

6.2 MEASURED LENS PATTERNS AT 0° ELEVATION SCAN

Antenna patterns were taken for four azimuth scan locations, namely, 0°, 15°, 30° and 45°. Appendix A includes azimuth and elevation measured patterns for 5.0, 5.3 and 5.6 GHz for each feed position.

The feed tilting and focusing adjustments were made to optimize the respective patterns at midband (5.3 GHz) in each scan location.

6.3 15° ELEVATION SCAN TEST SETUP

Appropriate cable lengths were added to scan the elevation beam 15° down toward the lens base. The feed spacer size was increased to position this scanned beam to the lens center.

A removable panel was designed into the line feed structure for direct access to the network of cables which connect the azimuth layers and elevation power divider. Figure 6-2 is a view of the feed with the panel removed.

Azimuth patterns were taken ±90° relative to the azimuth broadside 0° scan through the 15° scanned elevation beam. Again, the source was horizontally polarized. The upper azimuth and elevation tables were adjusted to locate the beam peak, and azimuth patterns were taken using the upper azimuth table control.

Elevation patterns were taken for the same polarization with the elevation mount control. All elevation patterns were taken referenced to the 0° broadside elevation scan for the ±45° sector.
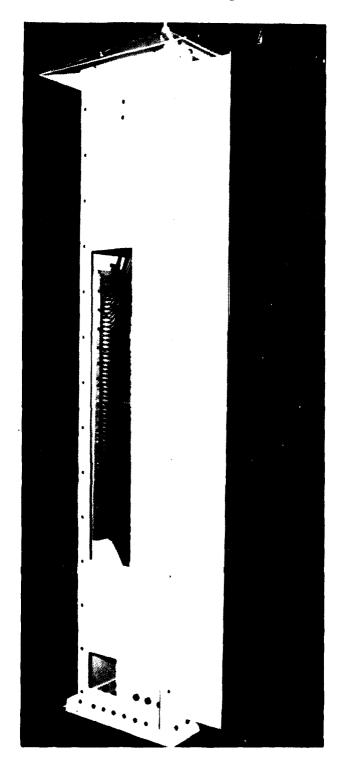
Figure 6-2.   Line Feed With Access Panel Removed

6.4 MEASURED LENS PATTERNS AT 15° ELEVATION SCAN

Azimuth and elevation patterns were measured for the 15° elevation scan case at two azimuth scan locations of the line feed: 0° and 30°. Appendix B includes the final measured results. All line feed tilting and focusing was adjusted to optimize the antenna performance at 5.3 GHz. Measurements were also taken at 5.0 and 5.6 GHz.

A discussion of the final antenna performance is included in the next section.

SECTION VII
SUMMARY AND CONCLUSIONS

7.1 ANTENNA PERFORMANCE

The wideband, wide-angle scan capability of the lens is well demonstrated in the measured patterns included in Appendix A and B. The antenna has been tested to both 45° azimuth scan at 0° elevation, and 30° azimuth simultaneously with 15° elevation beam scanning.

Test results have demonstrated that the lens can be scanned to wide azimuth angles ($\pm 45^\circ$) without pattern degradation over a 5.0 - 5.6 GHz band. The patterns confirm the design of the R-2R lens which provides a circular focal line and allows the patterns to remain perfectly focused for all azimuth angles.

The pattern tests also showed that the array can be scanned in elevation by displacing the line feed and scanning the line feed beam. No significant degradation of the elevation patterns was noted with elevation scanning.

The table below summarizes the antenna performance in the azimuth scan sector of $\pm 60^\circ$ relative to the on axis broadside beam location.

Freq. GHz	Scan Angle (Deg.) Az.	Elev.	Peak Sidelobe Level - dB	No. Sidelobes Exceeding dB 32	37	40
5.0	0	0	24.0	3	12	15
5.0	15	0	24.5	2	4	9
5.0	30	0	25.0	2	6	13
5.0	45	0	25.5	4	7	12
5.0	0	15	25.5	3	10	13
5.0	30	15	26.5	2	6	15
5.3	0	0	28.0	1	4	7
5.3	15	0	29.0	2	2	9
5.3	30	0	29.0	2	4	7
5.3	45	0	30.0	3	6	9
5.3	0	15	27.0	4	7	10
5.3	30	15	30.5	2	4	9
5.6	0	0	27.5	1	6	15
5.6	15	0	26.0	5	12	20
5.6	30	0	26.5	2	13	28
5.6	45	0	24.0	5	14	19
5.6	0	15	30.0	1	8	14
5.6	30	15	27.0	4	11	26
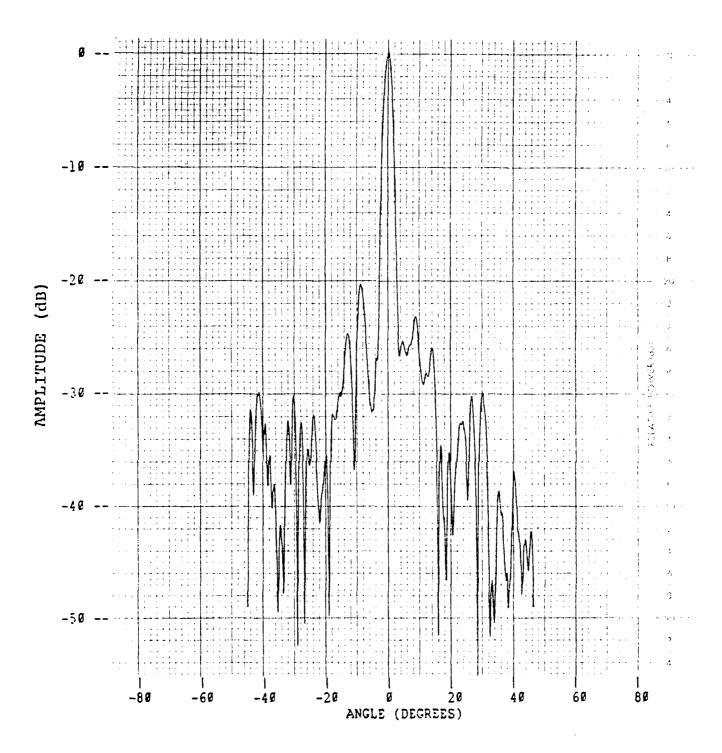
Figure A-11.   Elevation Pattern Cut at 5.3 GHz
15 Degrees Azimuth Scan
0 Degrees Elevation Scan
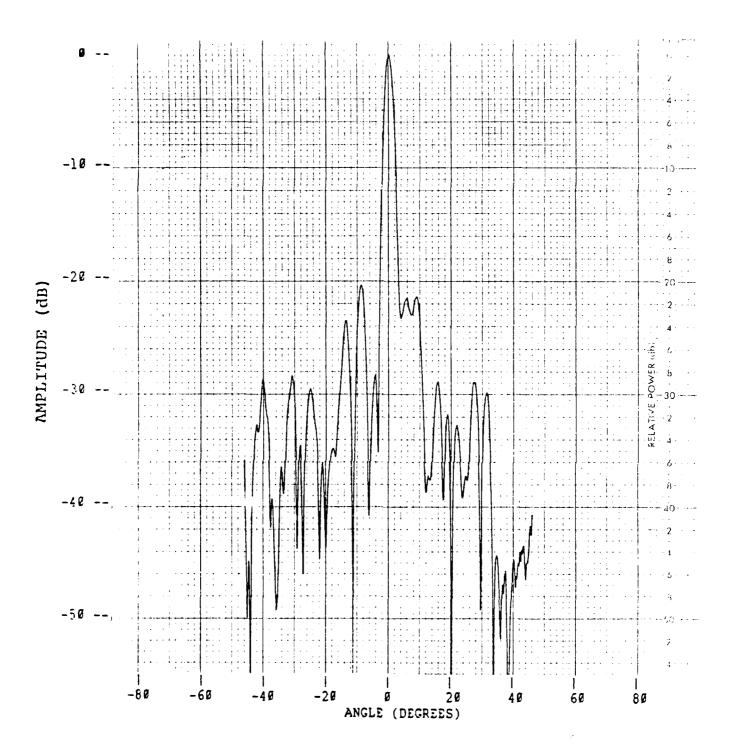
Figure A-10. Elevation Pattern Cut at 5.0 GHz
15 Degrees Azimuth Scan
0 Degree Elevation Scan

A-10
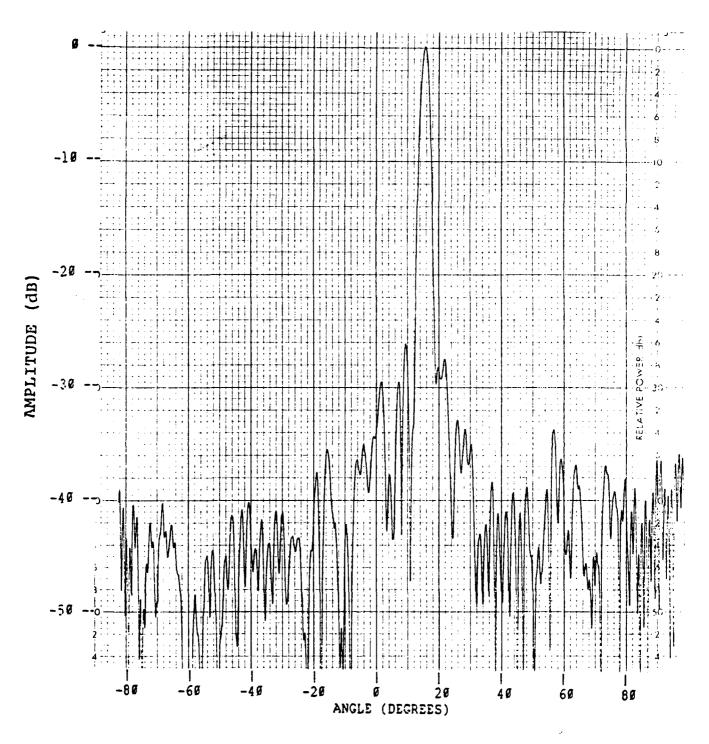
Figure A-9.   Azimuth Pattern Cut at 5.6 GHz
15 Degrees Azimuth Scan
0 Degree Elevation Scan
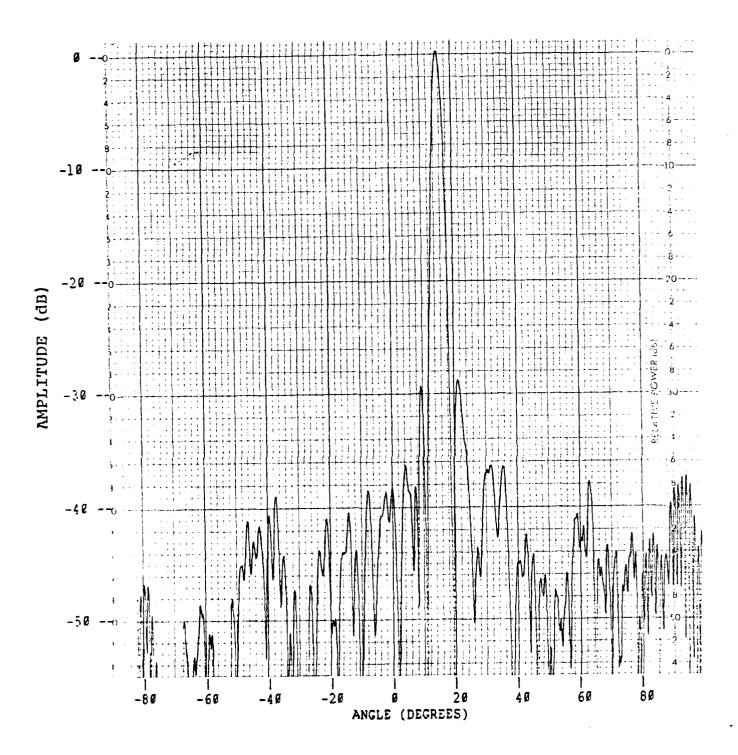
Figure A-8.   Azimuth Pattern Cut at 5.3 GHz
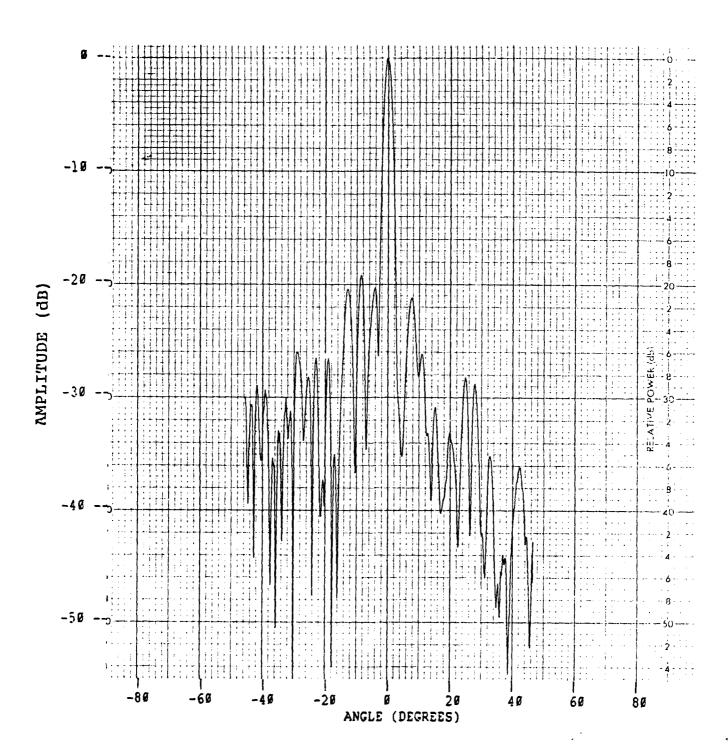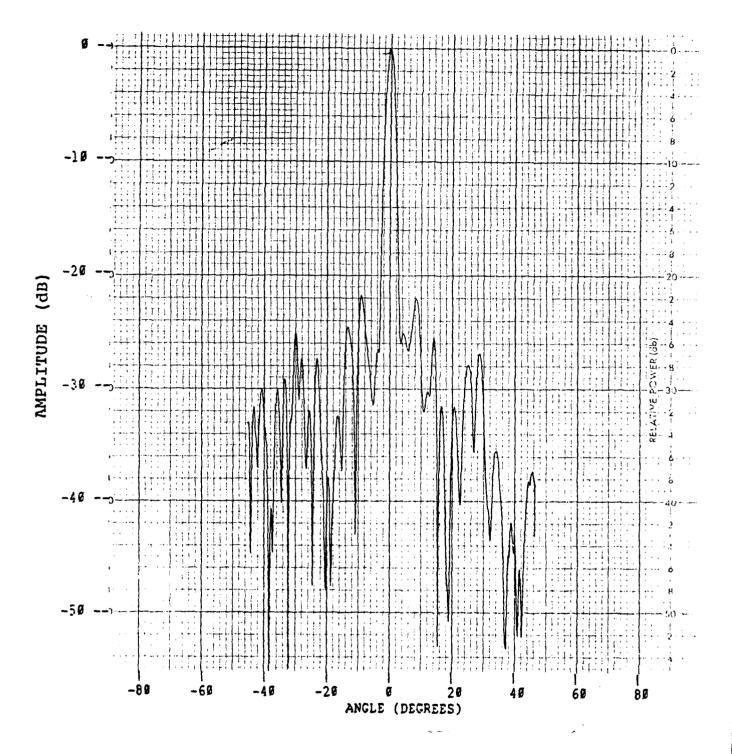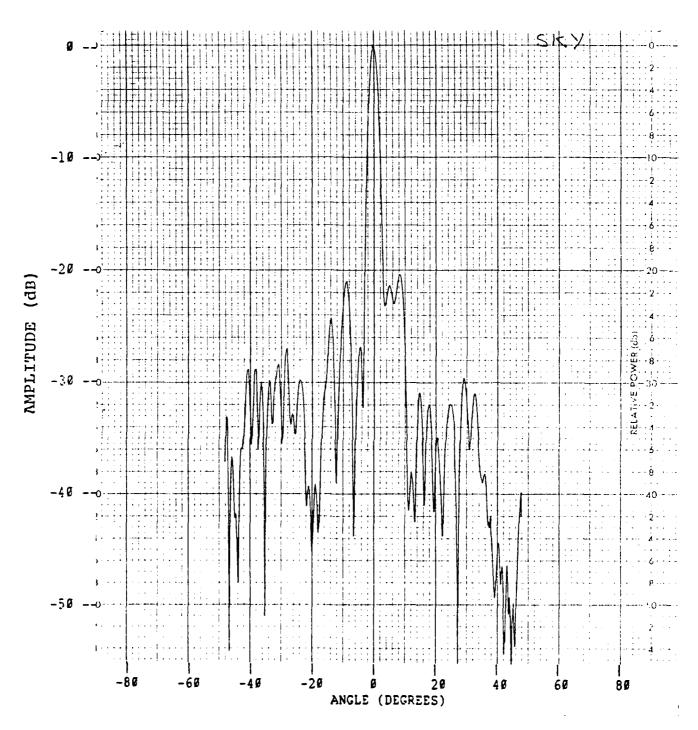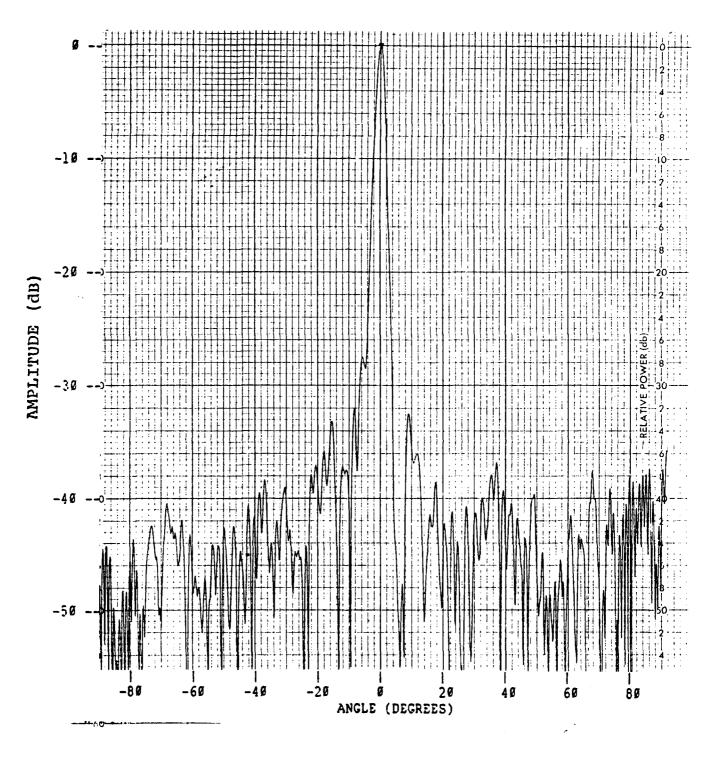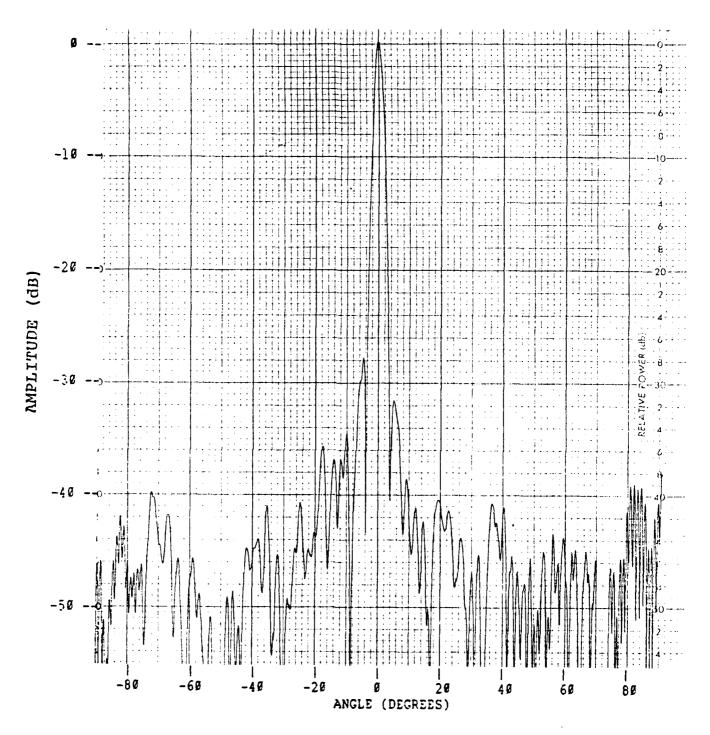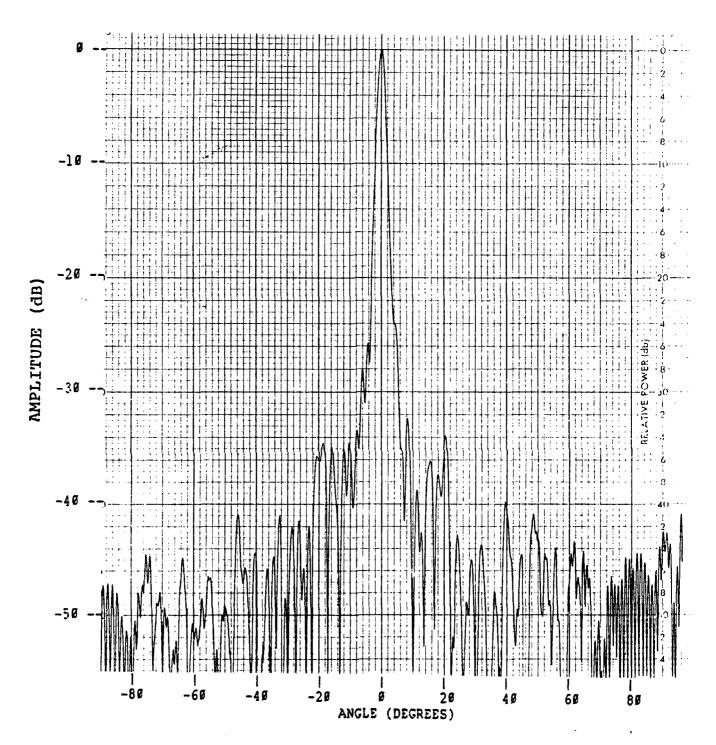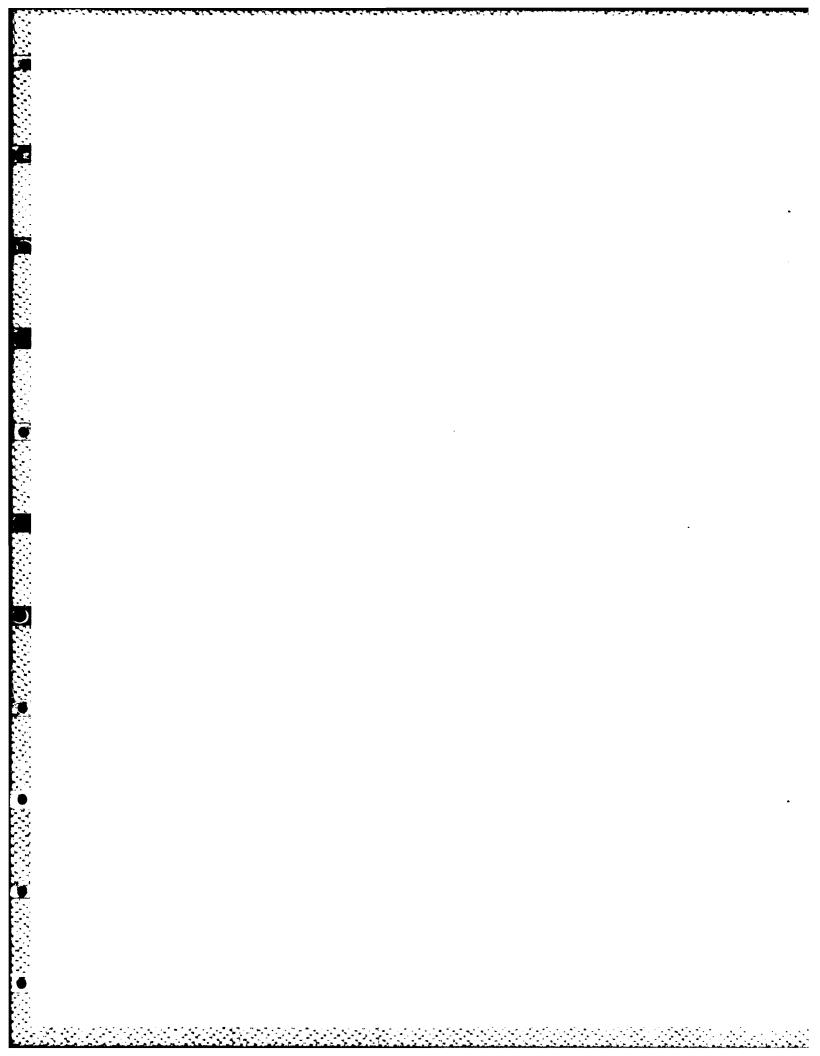15 Degrees Azimuth Scan
0 Degree Elevation Scan
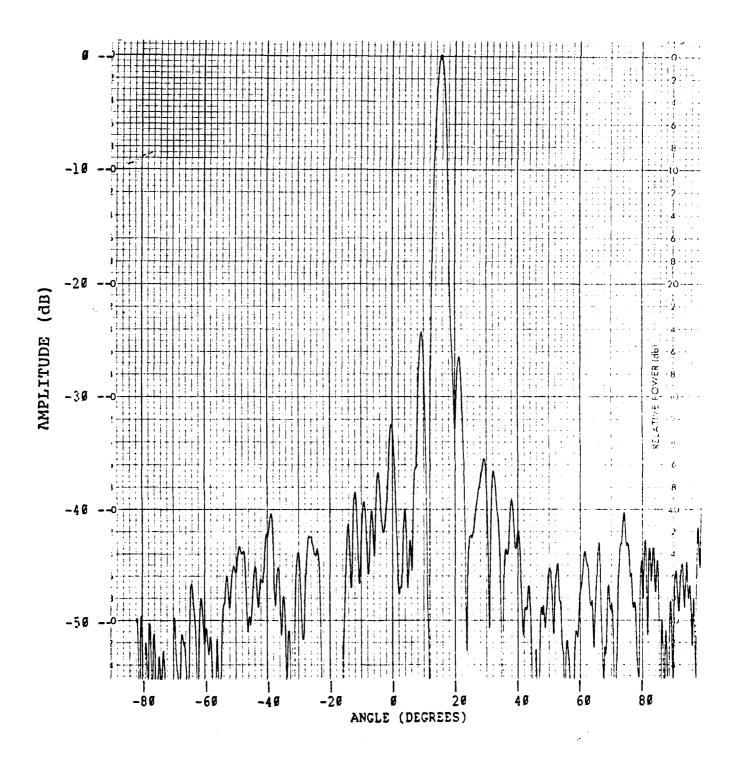
Figure A-7.   Azimuth Pattern Cut at 5.0 GHz
15 Degree Azimuth Scan
0 Degree Elevation Scan

Figure A-6.   Elevation Pattern Cut at 5.6 GHz
0 Degree Azimuth Scan
0 Degree Elevation Scan

Figure A-5. Elevation Pattern Cut at 5.3 GHz
0 Degree Azimuth Scan
0 Degree Elevation Scan

A-5

Figure A-4. Elevation Pattern Cut at 5.0 GHz
0 Degree Azimuth Scan
0 Degree Elevation Scan

Figure A-3.   Azimuth Pattern Cut at 5.6 GHz
0 Degree Azimuth Scan
0 Degree Elevation Scan

Figure A-2.   Azimuth Pattern Cut at 5.3 GHz
0 Degee Azimuth Scan
0 Degree Elevation Scan

Figure A-1. Azimuth Pattern Cut at 5.0 GHz
0 Degree Azimuth Scan
0 Degree Elevation Scan

APPENDIX A

LENS MEASUREMENTS 0° ELEVATION SCAN

Feed spillover outside of this region is not well attenuated by the lens absorber panels.

Considering the magnitude of the encountered phase variations in the lens microstrip layers, and the averaging and quantization correction technique used to trim the lens microstrip lines, final antenna performance has demonstrated feasability in attaining low sidelobe levels. Random phase errors are still present in the lens. Our best estimate is that the levels do not exceed $\pm 30^{o}$ peak and 10° RMS.

Since the low-range reflection test setup could not be used due to the weight of the assembled antenna, sidelobes below -40dB are known to be degraded by range reflections and are therefore not able to accurately measure. Although the previous table summary indicates a large number of sidelobes exceeding the 40 dB level, the measured patterns show most of them only exceed this level by a small margin.

Amplitude and phase assymmetries in the feed contribute to slight degradation in antenna performance at the band edges. It was possible to reduce sidelobe levels at the band edges, with small feed-position adjustments. However, the results were higher sidelobes at mid-band. Final pattern data has been presented, therefore to optimize lens performance at mid-band, and accept the poorer performance at the band edges.

The antenna performance in elevation was consistent for all scan conditions. Variations in the absolute phase between lens layers is as large as $\pm 35^{o}$. These phase errors could not be corrected in the lens microstrip line trimming.

7.2 CONCLUSIONS

The microstrip lens array approach is a good choice for wideband, wide-angle scanning. The major difficulties in attaining the low-sidelobe levels are in the manufacturing of the lens layers. Present available materials are not adequate for a microstrip lens. Fabrication techniques must be carefully implemented to meet the goals of this contract. Hazeltine has demonstrated that trimming of the lens microstrip is necessary, and that low sidelobes can be attained with suitable phase corrections. The trimming on the lens was limited by budgetary and time constraints so that -50 dB sidelobes were not expected.
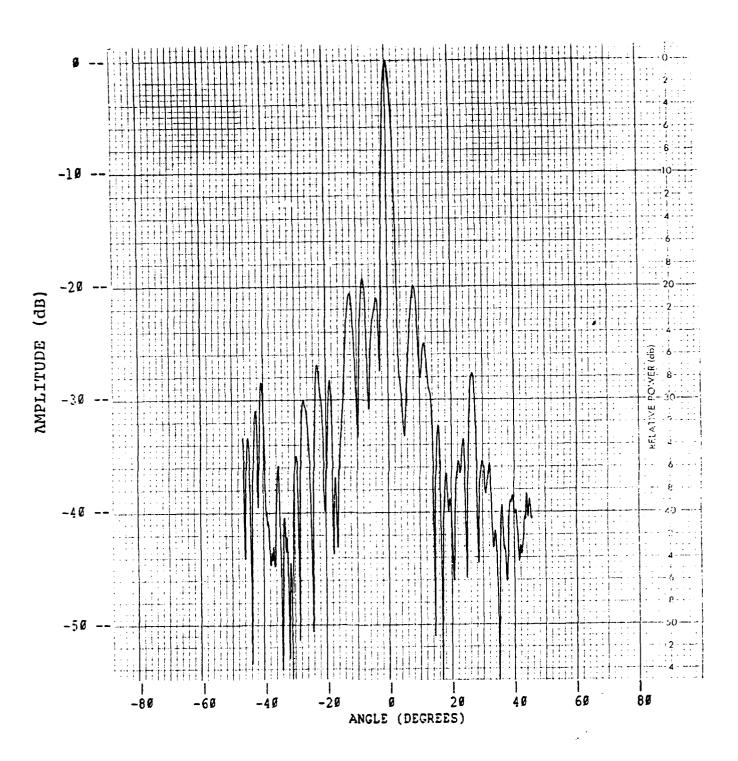
Figure A-12. Elevation Pattern Cut at 5.6 GHz
15 Degrees Azimuth Scan
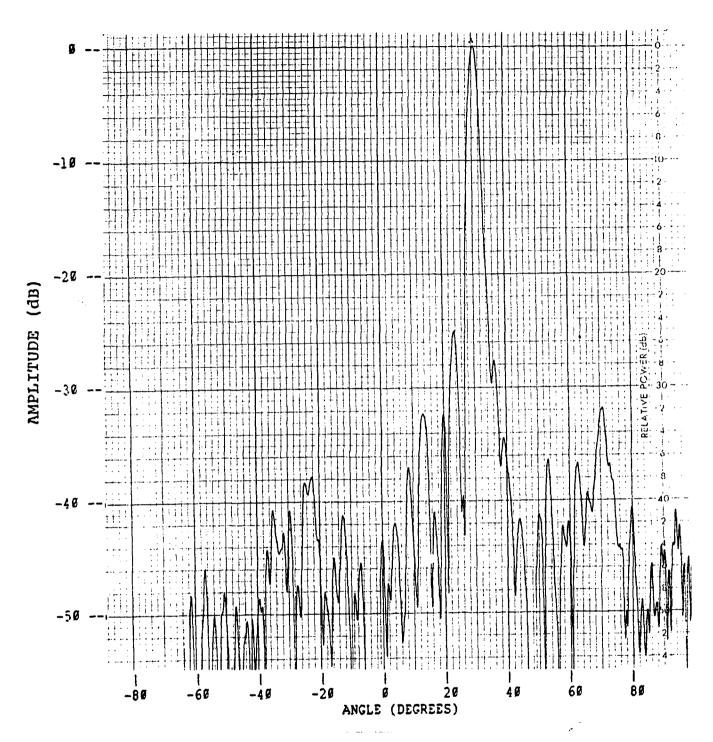0 Degrees Elevation Scan

Figure A-13.   Azimuth Pattern Cut at 5.0 GHz
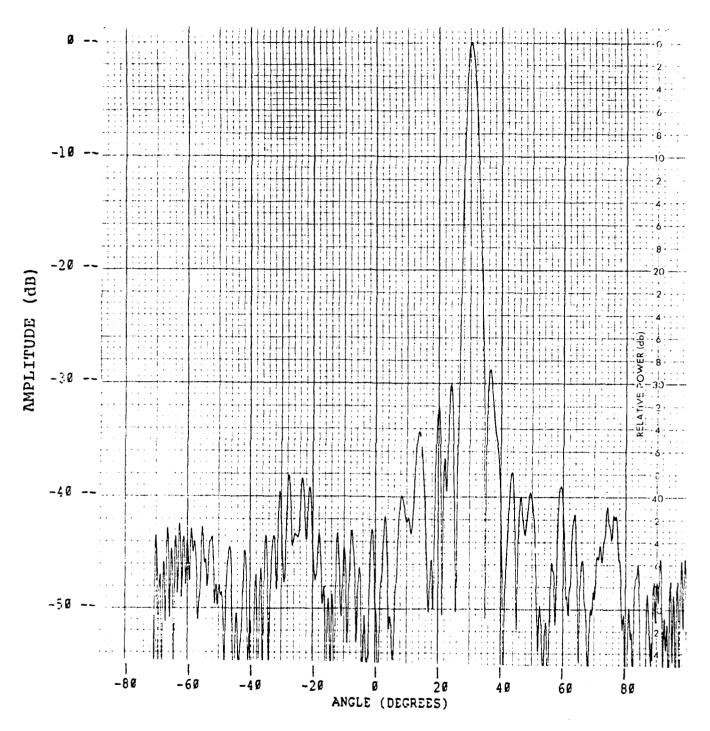30 Degrees Azimuth Scan
0 Degrees Elevation Scan

Figure A-14. Azimuth Pattern Cut at 5.3 GHz
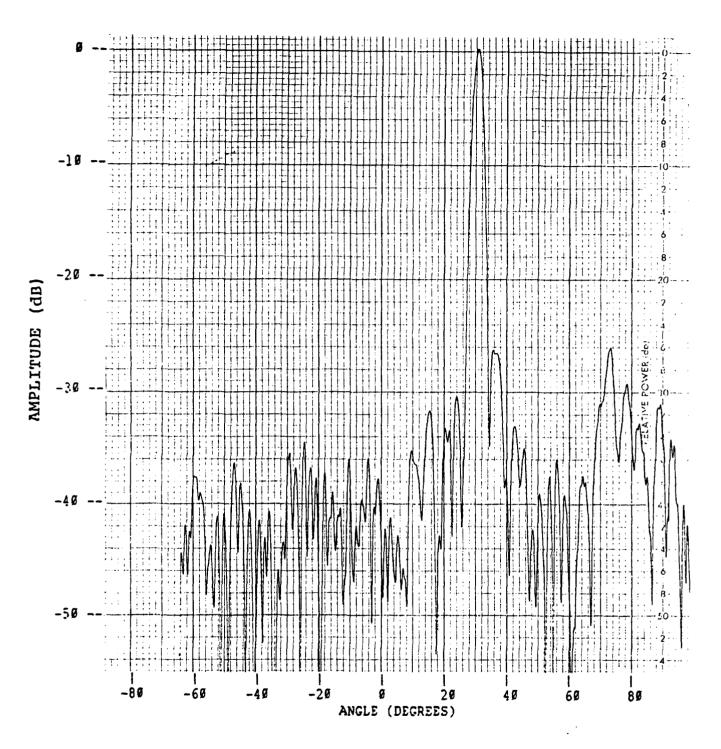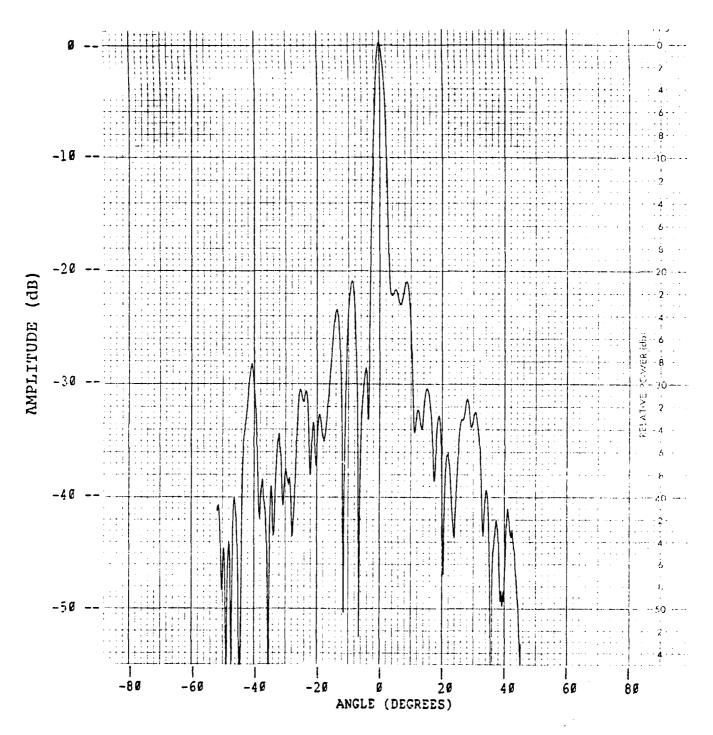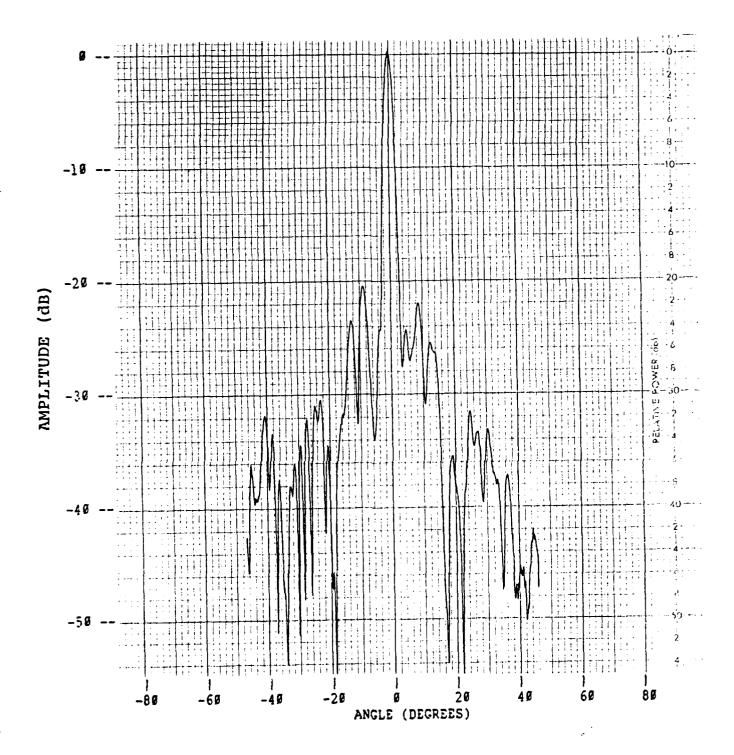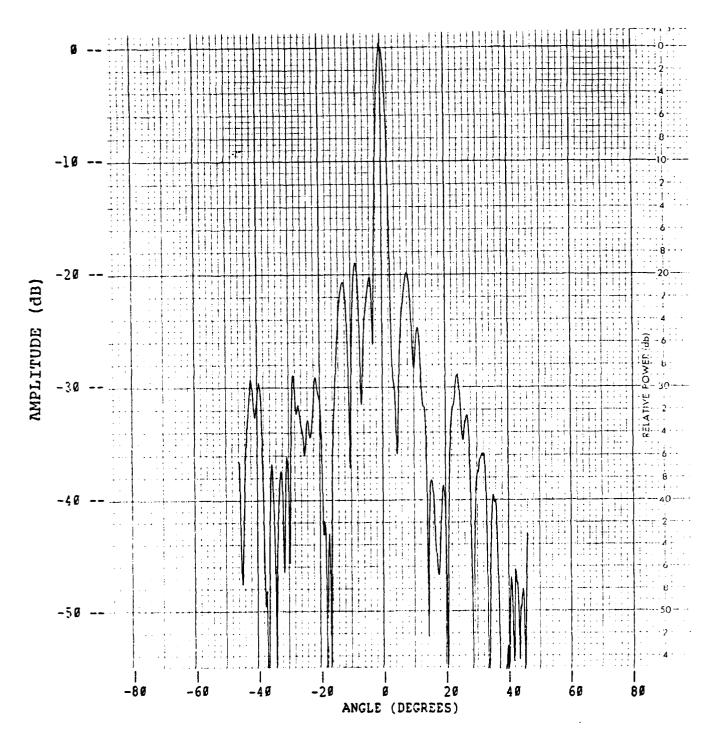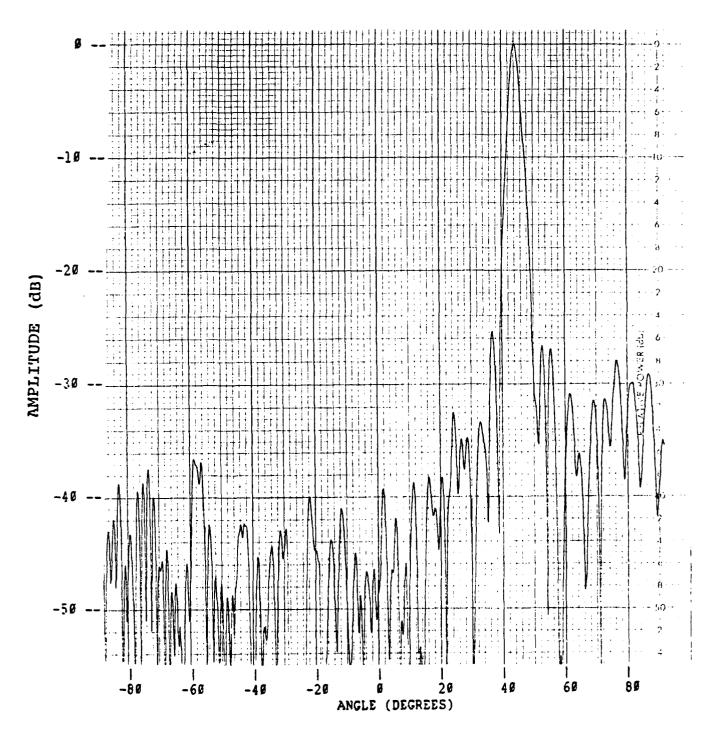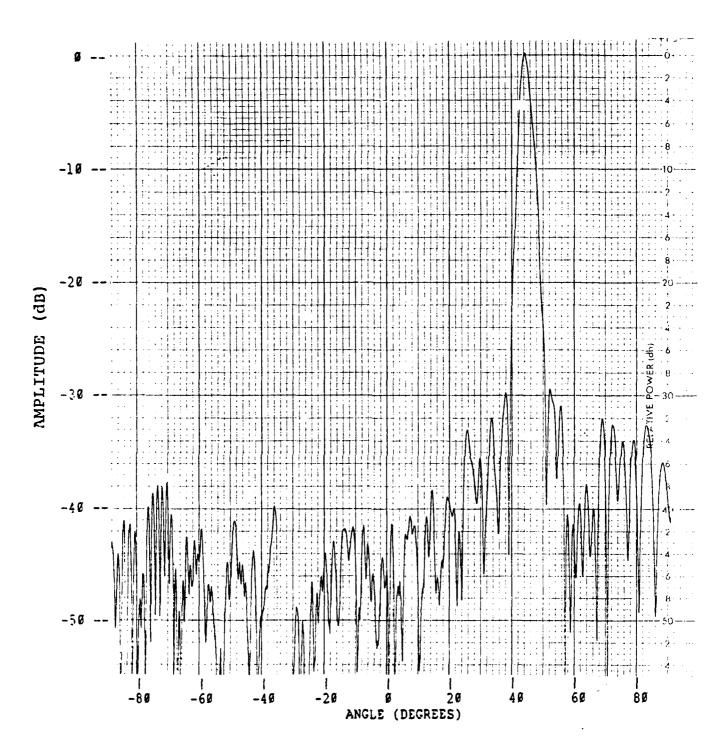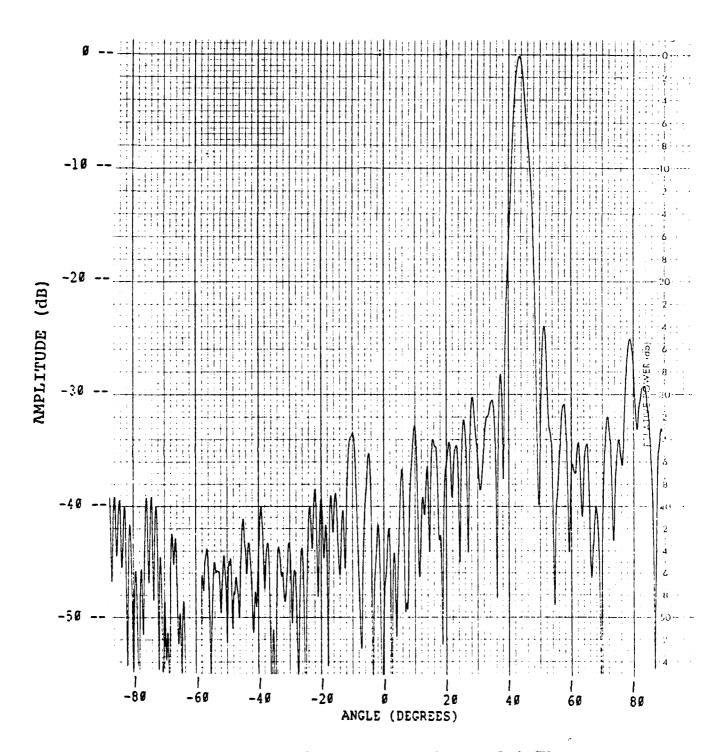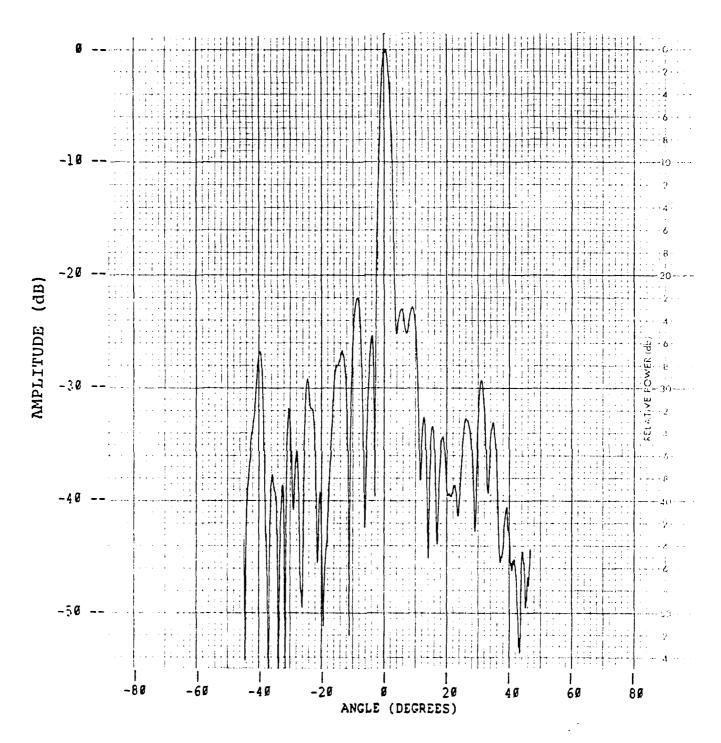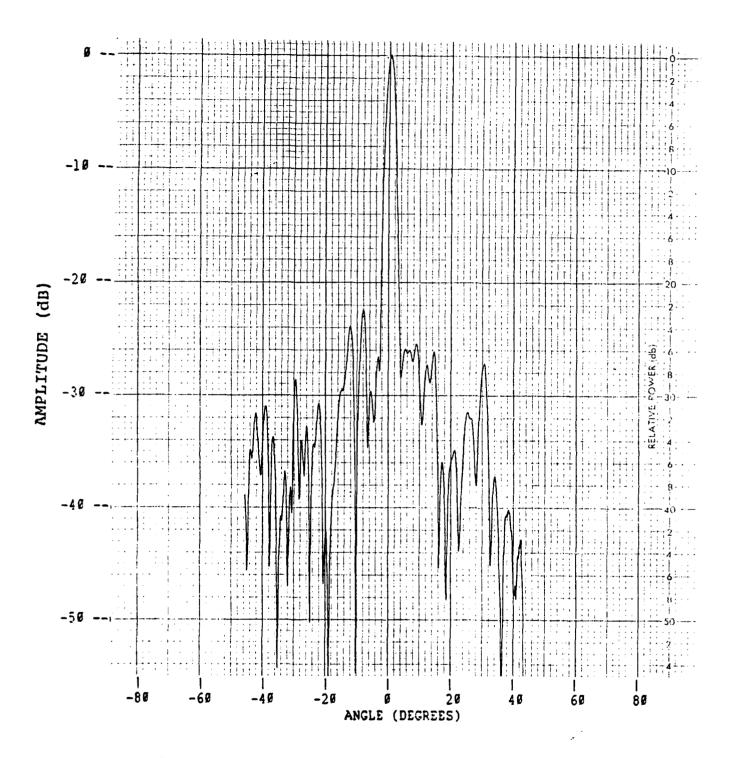30 Degrees Azimuth Scan
0 Degrees Elevation Scan

A-14

Figure A-15.   Azimuth Pattern Cut at 5.6 GHz
30 Degrees Azimuth Scan
0 Degrees Elevation Scan

Figure A-16.   Elevation Pattern Cut at 5.0 GHz
30 Degrees Azimuth Scan
0 Degrees Elevation Scan

Figure A-17. Elevation Pattern Cut at 5.3 GHz
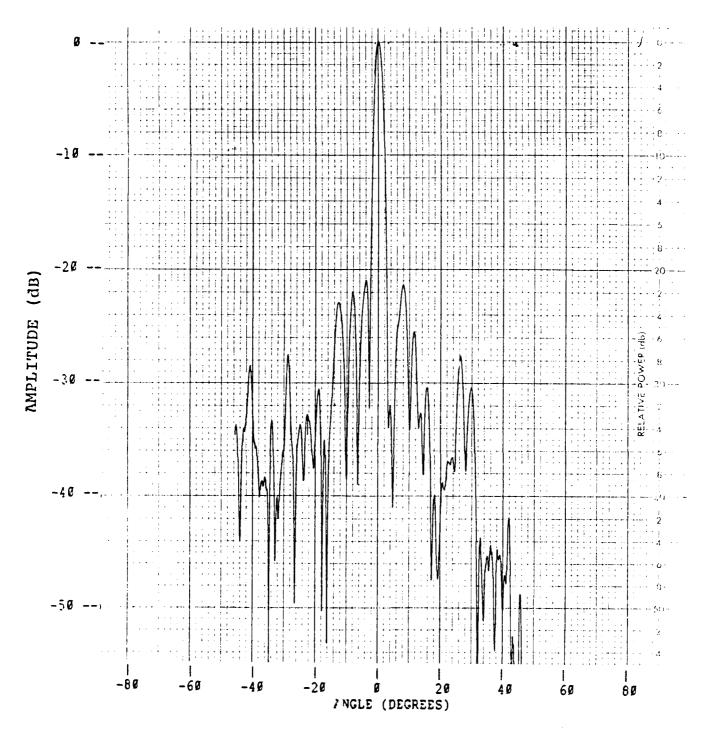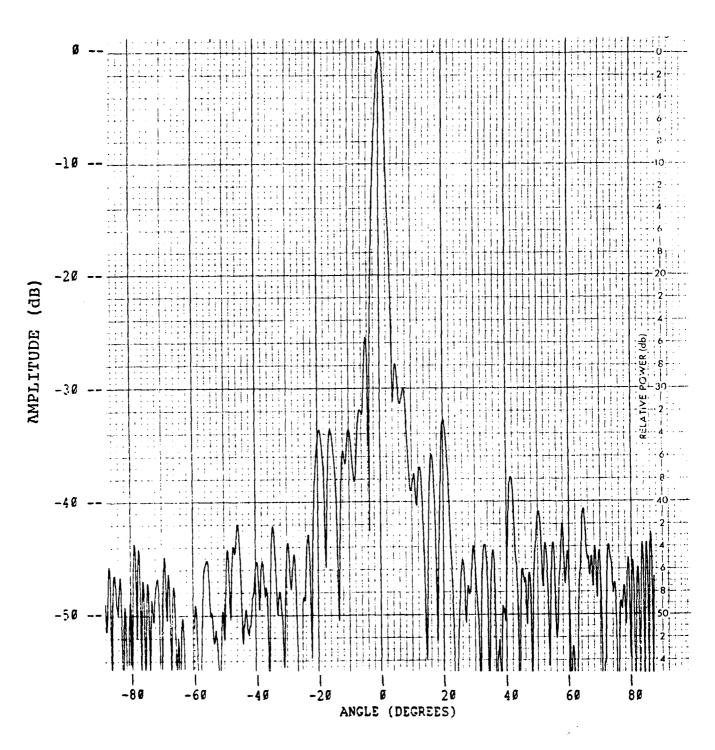30 Degrees Azimuth Scan
0 Degrees Elevation Scan

A-17

Figure A-18.   Elevation Pattern Cut at 5.6 GHz
30 Degrees Azimuth Scan
0 Degrees Elevation Scan

Figure A-19.   Azimuth Pattern Cut at 5.0 GHz
45 Degrees Azimuth Scan
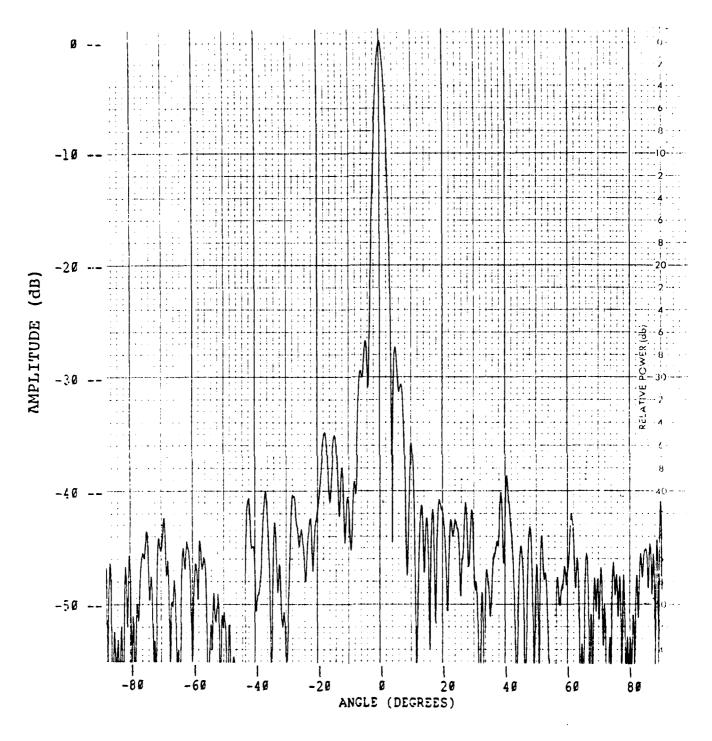0 Degrees Elevation Scan

Figure A-20.   Azimuth Pattern Cut at 5.3 GHz
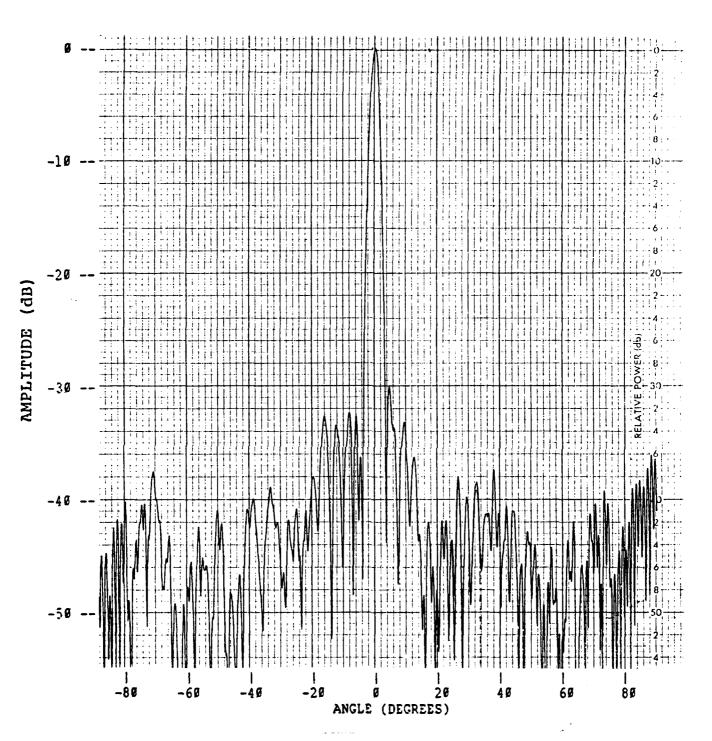45 Degrees Azimuth Scan
0 Degrees Elevation Scan

Figure A-21.   Azimuth Pattern Cut at 5.6 GHz
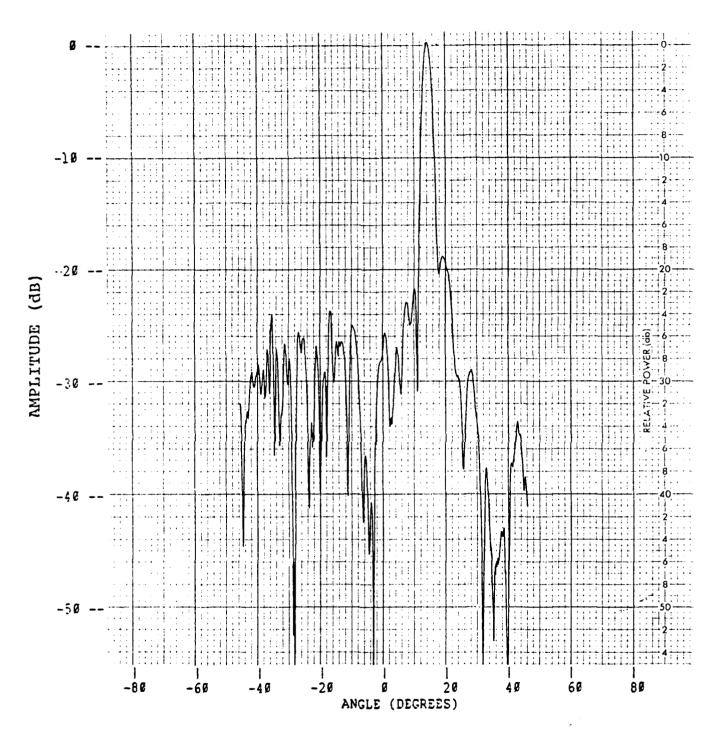45 Degrees Azimuth Scan
0 Degrees Elevation Scan

Figure A-22. Elevation Pattern Cut at 5.0 GHz
45 Degrees Azimuth Scan
0 Degrees Elevation Scan

Figure A-23. Elevation Pattern Cut at 5.3 GHZ
45 Degrees Azimuth Scan
0 Degrees Elevation Scan

Figure A-24. Elevation Pattern Cut at 5.6 GHz
45 Degrees Azimuth Scan
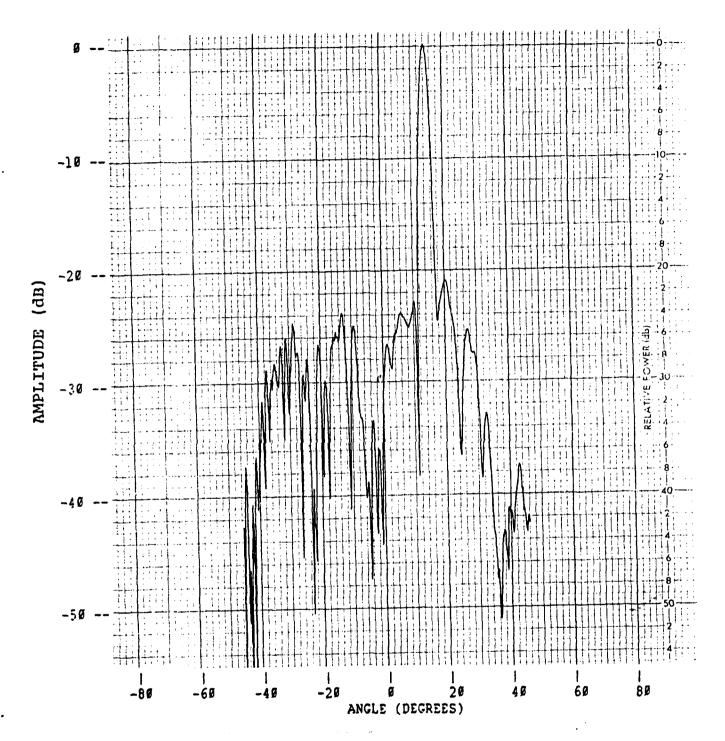0 Degrees Elevation Scan

APPENDIX B

LENS MEASUREMENTS 15° ELEVATION SCAN

Figure B-1.   Azimuth Pattern Cut at 5.0 GHz
0 Degrees Azimuth Scan
15 Degrees Elevation Scan

Figure B-2.   Azimuth Pattern Cut at 5.3 GHz
0 Degrees Azimuth Scan
15 Degrees Elevation Scan

Figure B-3.   Azimuth Pattern Cut ρ⁺ 5.6 GHz
0 Degrees Azimutn Scan
15 Degrees Elevation Scan

Figure B-4.   Elevation Pattern Cut at 5.0 GHz
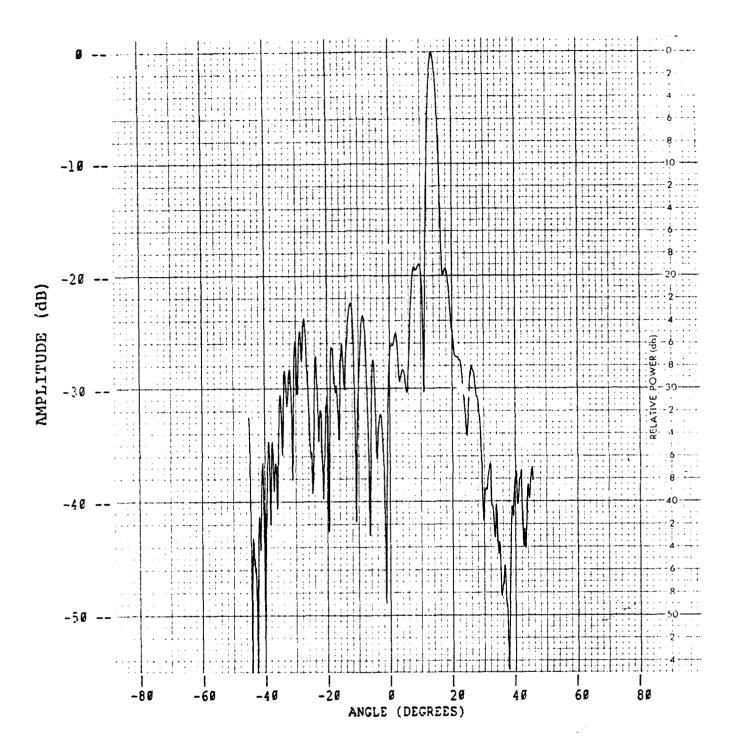0 Degrees Azimuth Scan
15 Degrees Elevation Scan

Figure B-5. Elevation Pattern Cut at 5.3 GHz
0 Degrees Azimuth Scan
15 Degrees Elevation Scan

Figure B-6.   Elevation Pattern Cut at 5.6 GHz
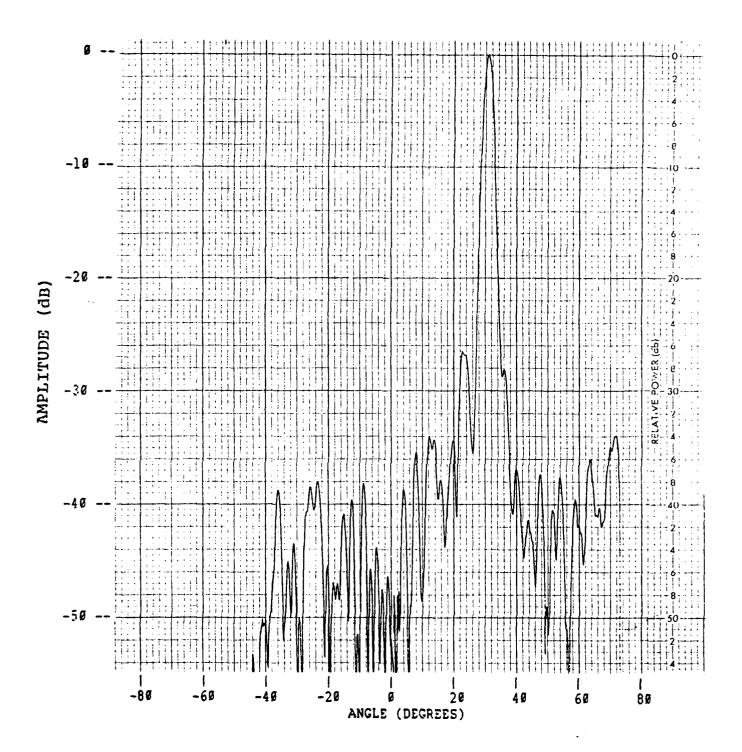0 Degrees Azimuth Scan
15 Degrees Elevation Scan

Figure B-7.   Azimuth Pattern Cut at 5.0 GHz
30 Degrees Azimuth Scan
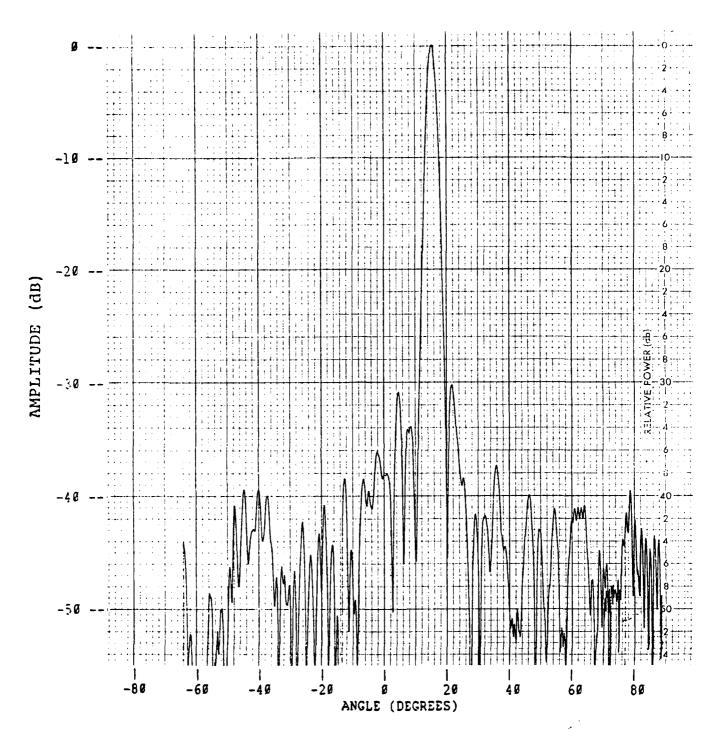15 Degrees Elevation Scan

Figure B-8.   Azimuth Pattern Cut at 5.3 GHz
30 Degrees Azimuth Scan
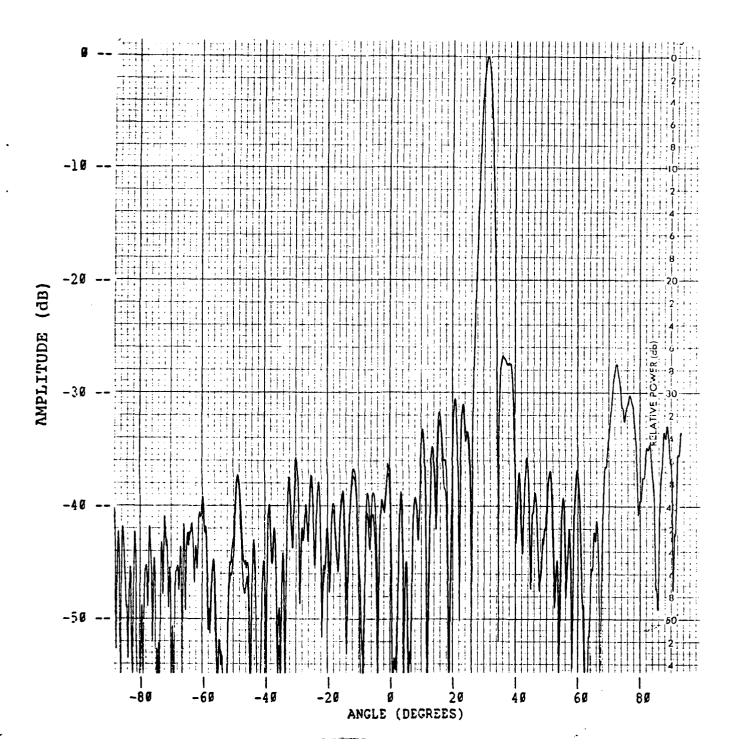15 Degrees Elevation Scan

Figure B-9. Azimuth Pattern Cut at 5.6 GHz
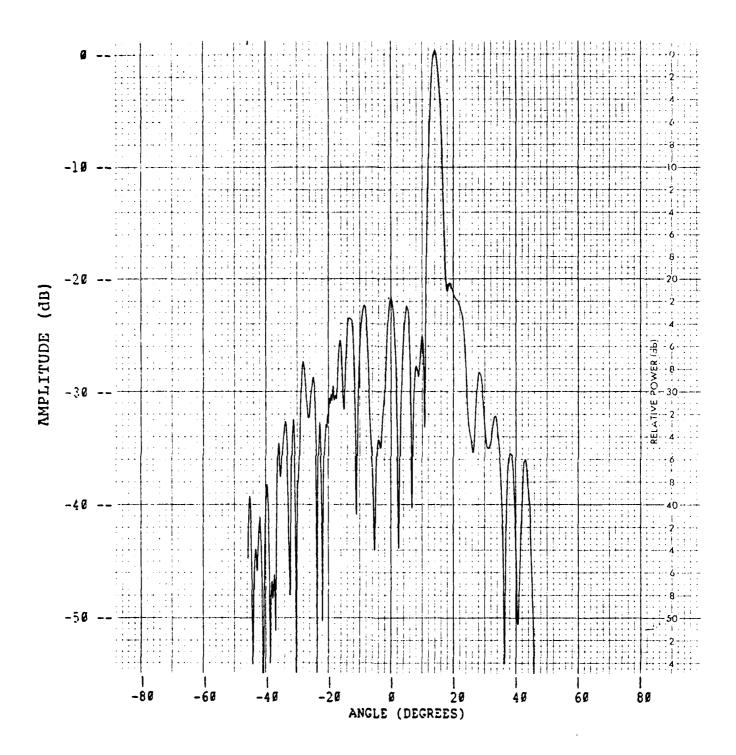30 Degrees Azimuth Scan
15 Degrees Elevation Scan

Figure B-10. Elevation Pattern Cut at 5.0 GHz
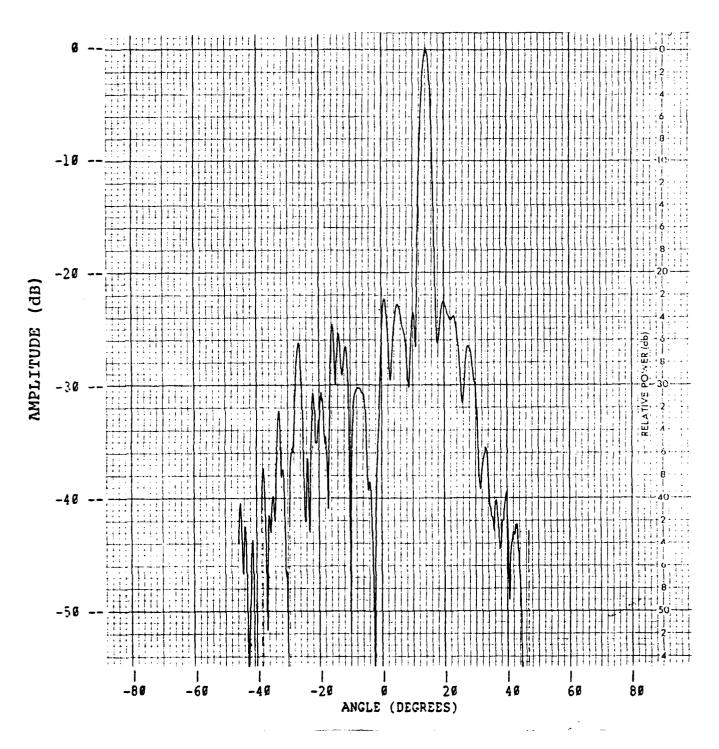30 Degrees Azimuth Scan
15 Degrees Elevation Scan

Figure B-11. Azimuth Pattern Cut at 5.3 GHz
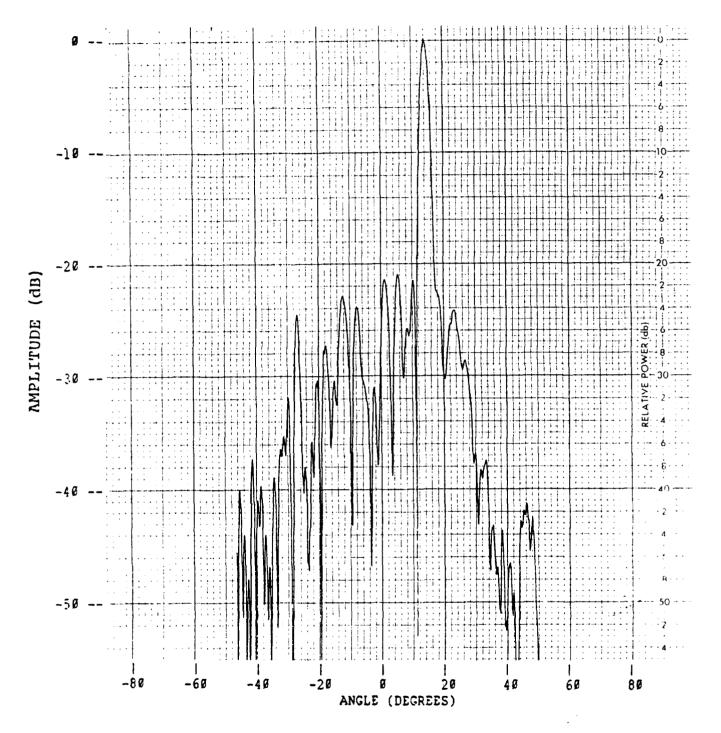30 Degree Azimuth Scan
15 Degrees Elevation Scan

Figure B-12.   Elevation Pattern Cut at 5.6 GHz
30 Degrees Azimuth Scan
15 Degrees Elevation Scan

MISSION
of
Rome Air Development Center

RADC plans and executes research, development, test and selected acquisition programs in support of Command, Control, Communications and Intelligence (C^3I) activities. Technical and engineering support within areas of competence is provided to ESD Program Offices (POs) and other ESD elements to perform effective acquisition of C^3I systems. The areas of technical competence include communications, command and control, battle management, information processing, surveillance sensors, intelligence data collection and handling, solid state sciences, electromagnetics, and propagation, and electronic, maintainability, and compatibility.

END

FILMED

8-85

DTIC